Soil diversity at Jezero crater and Comparison to Gale crater, Mars

A. Cousin, Pierre-Yves Meslin, O. Forni, Olivier Beyssac, E. Clavé, E. Hausrath, Pierre Beck, Erwin Dehouck, S. Schröder, Thierry Fouchet, et al.

Icarus 425 (2025) 116299

Contents lists available at ScienceDirect

Icarus

journal homepage: www.elsevier.com/locate/icarus

Research Paper

Soil diversity at Jezero crater and Comparison to Gale crater, Mars

A. Cousin [a,*], P.-Y. Meslin [a], O. Forni [a], O. Beyssac [b], E. Clavé [c], E. Hausrath [d], P. Beck [e], E. Dehouck [f], S. Schröder [c], T. Fouchet [g], C. Bedford [h], J. Johnson [i], P. Pilleri [a], J. Lasue [a], O. Gasnault [a], N. Martin [h], B. Chide [a], A. Udry [d], R. Sullivan [j], A. Vaughan [k], I. Poblacion [l], G. Arana [l], J.M. Madariaga [l], S. Clegg [m], S. Maurice [a], R.C. Wiens [h]

[a] Institut de Recherche en Astrophysique et Planétologie, Université de Toulouse 3 Paul Sabatier, CNRS, CNES, 31400 Toulouse, France
[b] Institut de Minéralogie, de Physique des Matériaux et de Cosmochimie, CNRS, Sorbonne Université, Muséum National d'Histoire Naturelle, 75005 Paris, France
[c] Deutsches Zentrum für Luft- und Raumfahrt (DLR), Institute of Optical Sensor Systems (OS), Berlin, Germany
[d] Department of Geoscience, University of Nevada, Las Vegas, NV, USA
[e] Institut de Planétologie et Astrophysique de Grenoble, CNRS, Université Grenoble Alpes, 38000 Grenoble, France
[f] Laboratoire de Géologie de Lyon : Terre, Université de Lyon, Université Claude Bernard Lyon1, Ecole Normale Supérieure de Lyon, Université Jean Monnet Saint Etienne, CNRS, 69100 Villeurbanne, France
[g] Laboratoire d'Etudes Spatiales et d'Instrumentation en Astrophysique, Observatoire de Paris-PSL, CNRS, Sorbonne Université, Université de Paris Cité, 92190 Meudon, France
[h] Earth, Atmospheric and Planetary Sciences, Purdue University, West Lafayette, IN, USA
[i] John Hopkins University Applied Physics Laboratory, Laurel, MD, USA
[j] CCAPS, Cornell University, Ithaca, NY, USA
[k] Apogee Engineering, LLC, Flagstaff, AZ, USA
[l] Univ. Basque Country UPV/EHU, 48940 Leioa, Spain
[m] Los Alamos National Laboratory (LANL), Los Alamos, NM, USA

ARTICLE INFO

Dataset link: http://pds-geosciences.wustl.edu/missions/msl/chemcam.htm, http://pds-geosciences.wustl.edu/missions/mars2020/supercam.htm, https://zenodo.org/records/13118478?preview=1&token=eyJhbGciOiJIUzUxMiJ9.eyJpZCI6IjIwYjNiMThkLTAzN2QtNDRkNi05M2E1LTlmNjhlZGIxNmVlNSIsImRhdGEiOnt9LCJyYW5kb20iOiI5MDc3ZTY3N2I1OWM1NDBmZGIyMjU0NjIyZTc1MTJmNSJ9.NFk2gCZ91D6s4Kcpto_2BESpXa1oV2nPVC64UUFy5Fo0TVoH4ScHU_bszyWhaS76NSnH4nA2mmTRxqTpUnYp9g

Keywords:
Mars
SuperCam
Mars2020
Perseverance
Soil

ABSTRACT

The martian soil is of particular interest as it can help us understand the different processes that have occurred on Mars by studying the chemistry and mineralogy of its constituents as a function of grain size. The fine-grained martian soil is thought to be homogeneous across the planet and thus to represent a global component. In this study we report on the soil targets analysed by the SuperCam instrument aboard the Perseverance rover, which is currently exploring Jezero crater. A total of 343 targets were analysed. Their grain size distribution confirms the sparsity of 250–900 Âµm particles in the martian soil, although both smaller and larger grains are present. We found that the local components, due to erosion of the local bedrock, are present not only in the very coarse grains or larger gravels of the soil, but also in the very fine ones (<250 Âµm). We detected some very coarse grains enriched in olivine, pyroxene and carbonate in both the crater floor and the delta front locations, whereas phyllosilicate-rich grains have been encountered only in the delta front. We have compared the Jezero fine-grained soil targets with those of Gale crater using ChemCam data. We found that those at Jezero show no evidence of Mg sulfates, in contrast to the observation at Gale. In addition, the fine-grained soil at Jezero is more hydrated than that at Gale, probably due to its higher specific surface area.

1. Introduction and objectives

The martian soil (Certini et al., 2020; Van Es, 2017) is formed through a variety of processes, such as physical and chemical alteration. Soil contains some dust component and are composed of various grain sizes, which indicate a range of mineral phases originating from local, regional, or even global sources due to wind transport and mixing (McSween et al., 2010; Yen et al., 2005). The martian soil is therefore often considered as representative of the bulk martian crust composition (Yen et al., 2005; Clark, 1993). Understanding the different mineralogies that constitute the martian soil can provide clues concerning the past

* Corresponding author.
E-mail address: agnes.cousin@irap.omp.eu (A. Cousin).

https://doi.org/10.1016/j.icarus.2024.116299
Received 19 February 2024; Received in revised form 29 August 2024; Accepted 3 September 2024
Available online 12 September 2024

environment, as the soil records the different aqueous alteration processes that Mars' surface has undergone. Moreover, better constraining the formation processes of the soil can help to better understand the different primary and secondary processes responsible for such phases. The study of the soil is also important to better constrain some modern processes, such as the exchanges between the surface and the atmosphere.

Bulk compositions of soil have been measured in situ at multiple landing sites (Viking1, Viking2, Mars Pathfinder, Spirit, Opportunity, Phoenix and Curiosity). Even though the analysis footprints of the instruments onboard are quite large, these missions revealed similarities in the chemical composition of the soil across the different locations (Yen et al., 2005; Ming et al., 2008; Meslin et al., 2013; O'Connell-Cooper et al., 2017), with components mixed between igneous minerals and secondary products (Rogers and Aharonson, 2008; Yen et al., 2005). Soil has been found to be enriched (compared to bedrock) in Cl, H and S (Yen et al., 2005). Some sulfate and chlorine salts have been detected in all of the landing sites (Clark, 1993; Arvidson et al., 2010; Yen et al., 2005; Rampe et al., 2018; David et al., 2022), as well as some perchlorates at the Phoenix landing site (Kounaves et al., 2014) and oxychlorine compounds at Gale crater (Leshin et al., 2013). At Gale crater, the mineralogy of soil targets sieved to < 150 μm has been explored for the first time by the CheMin and SAM instruments. CheMin uses the XRD technique (Blake et al., 2012) and SAM includes a quadrupole mass spectrometer, a tunable laser spectrometer, and a six-column gas chromatograph (Mahaffy et al., 2012) - that are used on the same powder as CheMin. These analyses showed that the < 150 μm soil grain size was mostly composed of a mixture of primary igneous phases (40.8 wt% plagioclase, 22.4 wt% olivine, 14.6 wt% augite, and 13.8 wt% pigeonite), minor phases include magnetite, hematite, anhydrite and some quartz; around 30 % of the material was seen as amorphous with the XRD technique (Blake et al., 2013; Rampe et al., 2018).

The ChemCam instrument, onboard Curiosity was the first to use the LIBS (Laser-Induced Breakdown Spectroscopy) technique on Mars, analysing for the first time the martian soil at a very fine scale (its LIBS spot size is 350–550 μm depending on the focus distance Maurice et al., 2012) and therefore several studies have used ChemCam LIBS to investigate the chemistry and inferred mineralogy of soil grains (Meslin et al., 2013; Cousin et al., 2015, 2017b; David et al., 2022). Meslin et al. (2013) and Cousin et al. (2015) have shown that the coarsest components were from local inputs, whereas the finer ones (<500 μm, e.g., smaller than the laser spot size) originated more globally. David et al. (2022) also showed the presence of hydrated sulfates in the amorphous component of the fine-grained soil in the lowest part of Gale crater, the source of which still needs to be understood, e.g., whether or not it is sourced from the sulfate unit of Mount Sharp (Fraeman et al., 2016; Rapin et al., 2021).

The Perseverance rover has been exploring Jezero crater since early 2021 (Farley et al., 2020). The rover explored the crater floor during the first 1.5 years of the mission (Sun et al., 2023). The Máaz and Seítah units revealed some unexpected terrains, with a succession of several lava flows in Máaz (Wiens et al., 2022; Farley et al., 2022; Udry et al., 2022), and an olivine-rich cumulate in Seítah (Wiens et al., 2022; Farley et al., 2022; Beyssac et al., 2023b; Liu et al., 2022). Perseverance also explored the delta front (Williams et al., 2023) and the delta itself. soil targets have been investigated both during the crater floor and the delta front campaigns.

At Jezero, Vaughan et al. (2023) used the MastCam-Z (Bell et al., 2021) multispectral data to investigate the different types of soil depending on their mineralogy, and the different imagers to study the texture of the soil, such as grain sizes and roundness, up to sol 350. Hausrath et al. (2023) described some aspects of the soil observed in the floor of Jezero Crater, focusing on the surface–atmosphere interactions, and showed that some crusts can form at the surface. In the context of Mars Sample Return (MSR), a soil sample was acquired and stored in its sample return tube at Observation Mountain, which is a megaripple (samples called Atmo_Mountain and Crosswind_Lake), and its description is published in Hausrath et al. (2023). Detailed in-situ soil analyses are therefore important for a better context and a more representative understanding of this sample.

The remote-sensing SuperCam instrument (Wiens et al., 2021; Maurice et al., 2021; Fouchet et al., 2022) has used three techniques to study soil in Jezero crater: LIBS (Laser-Induced Breakdown Spectroscopy), the VISIR (Visible and near InfraRed) reflectance spectroscopy and the Remote Micro Imager (RMI). VISIR spectroscopy is being used for the first time in-situ, allowing the first comparisons between orbital and in-situ observations. SuperCam is the second instrument using the LIBS technique on Mars, after ChemCam.

The aim of this study is to provide new insights into the formation processes of the Martian soil. Chemical and mineralogical compositions of the soil as a function of grain size and rover localization are therefore investigated.

All soil targets analysed by SuperCam LIBS and VISIR techniques up to the MSR soil sample acquisition (sol 650) have been explored. SuperCam can perform observations rapidly around the rover, allowing a large number of observations to be done in order to perform several statistical analyses such as chemistry and mineralogy as a function of grain size, and as a function of rover location. The LIBS technique returns spectra containing all the emission lines for the elements present in the target, allowing elemental compositions to be determined. Comparing these spectra acquired at Jezero to those acquired at Gale crater can shed light about the similarities or differences between the fine-grained soil observed at both landing sites, even for non-quantified elements. Indeed, the two instruments not only share the same technique; they are very similar in design, and both have a sub-millimetric spot-size analysis. By investigating the fine-grained soil (<250 μm Wentworth, 1922) analysed at Gale crater by ChemCam and those analysed at Jezero crater by SuperCam, a direct comparison between the two sites can be done and the hypothesis of the global homogeneity of the fine-grained soil can be further tested.

2. Methodology

2.1. SuperCam instrument

The SuperCam instrument onboard Perseverance is a combination of five different remote-sensing techniques: Laser-Induced Breakdown Spectroscopy (LIBS), Raman, and VISIR spectroscopy, along with a microphone and a colour camera. The instrument is made of three parts: the Mast Unit (containing the laser, telescope, RMI camera, infrared spectrometer, electronics), the Body Unit (three spectrometers from UV to near infrared) and the Calibration targets located on the rover deck. More details about the instrument can be found in Wiens et al. (2021), Maurice et al. (2021), Manrique et al. (2020) and Cousin et al. (2022c). The synergy from the combination of techniques is of great interest to investigate the mineralogy, structure, chemistry, physical parameters as well as textural context of the remotely analysed targets. Raman spectroscopy can be performed up to around 5 m away, LIBS up to 10 m and VISIR and imaging up to infinity.

The LIBS technique is very similar to that of the ChemCam instrument onboard the Curiosity rover (Maurice et al., 2012; Wiens et al., 2012). It consists of a pulsed 1064 nm Nd-YAG laser, with a spot size varying from 160 μm at 2 m to 450 μm at 7 m (Maurice et al., 2021). From this technique, the chemical composition of the target can be assessed and is reported as eight major-element oxides (SiO_2, TiO_2, Al_2O_3, FeO, MgO, CaO, Na_2O and K_2O) (Anderson et al., 2021). H, S and Cl elements could also be considered as major elements as they are found at more than 1 wt% in soil (O'Connell-Cooper et al., 2017; Yen et al., 2005). These elements can be detected by SuperCam but are not yet quantified, such as most of the minor and trace elements. However, Ba, Li, Sr, Cr, Mn quantification is under progress (Gabriel

et al., 2023). The microphone is used for each LIBS analysis to provide physical properties (i-e, hardness) of the target when possible (Chide et al., 2020).

The RMI uses a CMOS camera of 2048x2048 pixels, with an angular size of 10 μradians and a resolution of 50 μradians (Gasnault et al., 2021). The camera gives therefore information about the pointing for each of the techniques, along with the textural and morphological information of the target, as shown in Mangold et al. (2021).

The Raman technique uses a 532 nm pulsed laser and has a shift range from 150 cm^{-1} to > 4000 cm^{-1}. This technique is used to identify major mineralogies, when sampling a relatively pure crystal. Mixture of small phases will decrease the signal-to-noise ratio until no mineral phases can be distinguished. Indeed, the Raman spot size analysis varies from 1.5 mm for a target at 2 m, up to 5.2 mm for a target at 7 m, which therefore is larger than the LIBS spot size. Therefore, the Raman technique is rarely used in soil targets, as the spot size corresponds to a mixture of several different grains, with no signal as a consequence.

The VISIR spectroscopy uses the reflection of sunlight to analyse the frequencies of molecule bond vibrations on a target surface. From the analysis of these vibrations, some of the minerals present in the target can be determined. SuperCam's VISIR technique has several spectral regions: the VIS part from 379–464 nm and 535–855 nm, using the VIO and transmission spectrometers (Wiens et al., 2021), and the IRS (Infrared Spectroscopy) part in the 1.3–2.6 μm range, that uses an Acousto-Optic Tunable Filter (AOTF) spectrometer to acquire the spectrum of reflected light. The field of view for the VISIR technique is 0.75 mrad at wavelengths < 1 μm and 1.15 mrad at wavelengths > 1.3 μm. Therefore the analytical footprint is around 1.4–2.3 mm for a target at 2 m, and up to 5–8 mm for a target at 7 m. Therefore, the VISIR field of view is larger than that of the LIBS (160 μm at 2 m to 450 μm at 7 m). Description of this specific IRS technique is given in Fouchet et al. (2022).

Spectral observations are made at individual points on the targets, with each observation sequence consisting of a raster of between three and ten points in a line or grid pattern. The spacing of the rasters can be adjusted, but is normally 1–5 mm between points. The instrument is focused on the target for the initial point, and is refocused for the final point; focus activities are sometimes spaced throughout the raster, depending on the spacing and local topography of the target.

The LIBS observations use a number of laser shots per point; in most cases 50 shots have been performed in soil, even though in some targets only 30 shots were used (the norm for rocks), such as in rasters that included both rocks and soil. LIBS compositions normally combine the results of these shots into a single average spectrum per point. However, each laser shot creates a shock wave that expels the fine-grained material and dust (David et al., 2021). Therefore, each LIBS shot samples a new set of grains. Therefore, single-shot spectra (instead of average spectra) are used for many aspects of soil observations.

The VISIR observations are acquired before the LIBS technique in soil. In doing so, the VISIR field of view is composed of a mixture of grains that have not been moved away by the LIBS laser shock wave. When preparing the activities, VISIR observations are planned when the target is in sunlight, avoiding shadows.

Instrument details can be found in Wiens et al. (2021) and Maurice et al. (2021). This study uses data from the LIBS and VISIR techniques, along with RMI images for the context and grain size assessment.

2.2. VISIR data analysis

The calibration of the radiometric response of the IRS technique was performed shortly after landing (Royer et al., 2023), using a dedicated onboard calibration target (the aluwhite target Manrique et al., 2020; Cousin et al., 2022c). For this study, several absorption bands along with spectral slopes have been investigated from soil spectra in order to assess the mineral compounds of the analysed targets. The same methodology from Viviano et al. (2014) has been used and adapted to SuperCam data, as explained in Royer et al. (2020). The presence of carbonates and/or Mg-OH phyllosilicates is inferred via the 2.32 μm band, carbonates via both the 2.32 and the 2.53 μm bands, molecular hydration with the 1.93 μm band, low-calcium pyroxene with the 1.81 μm band, and ferric oxides and/or oxyhydroxides via the 545 nm band. The 1.3–1.8 μm slope is used as a proxy for olivine.

2.3. LIBS data quantification and stoichiometric analyses

A spectral database of 334 targets has been used to quantify the SuperCam LIBS data from Mars. This database is a ChemCam heritage, e.g. built from the same samples used for the ChemCam database (Clegg et al., 2017). The SuperCam database has been acquired mainly at an instrument-sample distance of 3 m, using the Body Unit Flight Model and the Mast Unit Qualification Model. Both units were in a cold chamber (around −15 °C) and the targets were placed under Mars atmosphere [around 7 mbar of CO_2], at Los Alamos National Laboratory (Anderson et al., 2022). Major-element oxide compositions (MOC) from Mars targets are determined from multivariate tools developed using this spectral database. Details about models can be found in Anderson et al. (2022). Minor and trace elements (such as Rb, Sr, Ba, Cr, Mn, Zn, F, Li, Cu, Ni) as well as S, CL and H are not quantified yet (Gabriel et al., 2023) and therefore relative values are given for now. For most of these minor and trace elements this qualitative value is obtained by the peak area after fitting the line of interest, or by calculating a score (such as described in Meslin et al., 2022 for the Cl and S, respectively). The H signal is assessed by its ICA score (Meslin et al., 2022; Clavé et al., 2022). The SuperCam signature for Cl and S is really weak, especially in the shot-to-shot data, making the sensitivity very low. Therefore, when looking for correlations between Cl and/or S with other elements, only the point to point data (and not the shot-to-shot) will be used in order to increase the signal sensitivity.

When the grain size in the soil becomes sufficiently large, i.e., larger than the LIBS spot size (around 220 μm at 3 m), the laser may sample a single crystal. It is then possible to perform a stoichiometric analysis of this crystal from the MOC derived abundances. To test stoichiometric composition of plagioclase, olivine, and pyroxenes, we applied the series of criteria defined by Beyssac et al. (2023a) and Udry et al. (2022) for the crater floor units with only minor modification. We first identified the possible pure grains by applying these criteria to the entire MOC dataset. Then the same approach is used with the single-shot data to make sure that the point-averaged MOC composition that appears to be a single mineral does not coincidentally happen to be a mineral mixture, and that relevant elements (e.g., Fe, Mg, Si for olivine) are constant throughout the laser burst. If all criteria are met, then a stoichiometry is calculated for the point considered, assuming 4 oxygens for olivine and 6 for pyroxenes, and that all Fe is in the form Fe^{2+}.

Even though the ChemCam and SuperCam instruments are very similar in terms of their LIBS technique, their data quantifications depend on different databases developed in laboratory, as mentioned above for SuperCam (Chemcam's quantification details can be found in Clegg et al. (2017). Therefore there could be some possible biases inherent in each instrument and/or database, which has not been investigated yet. In order to compare the fine-grained soil observed with ChemCam and SuperCam, the Independent Component Analysis (ICA) technique is then used for qualitative comparisons.

The ICA technique is a multivariate tool used to classify different data sets such as LIBS spectra (Comon, 1994; Forni et al., 2013; Lasue et al., 2011). ICA identifies different statistically independent components among the data set, which allows us to sort the spectra depending on these components. These components are directly related to chemical elements (i-e they are close to a pure elemental spectrum). Covariance scores are then computed for each component. ICA scores are related but not linearly to the elemental contents. We have used in the study the Joint Approximate Diagonalization of Eigenmatrices (JADE) ICA algorithm (Cardoso and Souloumiac, 1993).

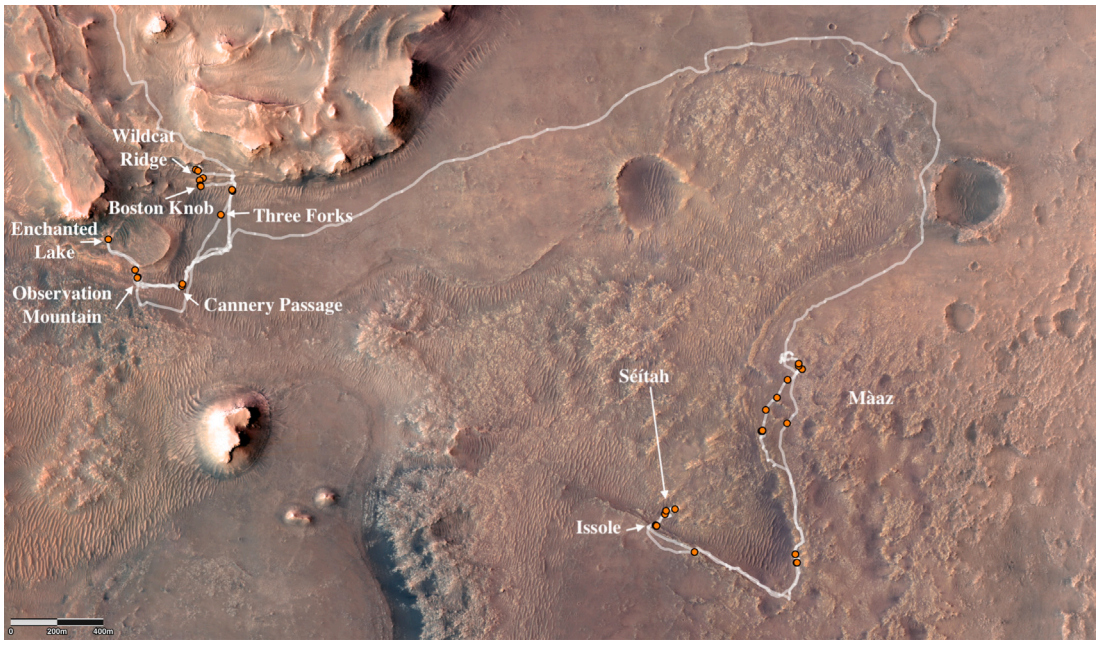

Fig. 1. Map of the rover traverse in the crater floor (grey line), with all the SuperCam soil targets highlighted with orange dots.

2.4. Data selection

Selection of the data for this study has been made following several steps: 1/ visual selection of points that sampled a soil target, 2/ quality assessment of the associated spectra, 3/ removing points for which a buried pebble has been identified.

The first part of the selection is made via visual inspection, using the RMI image of each LIBS SuperCam target. Rock-dedicated observations sometimes include points that sampled the soil. This is the case for example when the rock shows a depression that is filled with soil and dust, or when a few points missed the target. In this study, pockets of soil/dust on a rock have not been used, as it is difficult to make sure the rock beneath is not contributing to the signal. However, when some points missed the rock target, they have been taken into account when they corresponded to the first or the last one of the raster, as these are always associated to a focus activity, which maximizes the quality of the data. If another point among the raster missed the rock and fell into the soil, then we checked if there was a focus on that point. If yes, the data has been included in the study, otherwise it depends on several aspects: if this point is following a focused point that already sampled the soil (for example, point #2), it has been included in the study; if the point is occurring after a focus performed on the rock, then this point is discarded as the distance between the rock and the soil may be different enough to affect the LIBS signal quality.

Sometimes on coarse-grained soil (or heterogeneous ones) the LIBS points are not easy to spot. When in doubt (when the point is between pebbles, or when it is in shadow), the point is also discarded. soil targets are not classified according to their context deposit (whether or not they are part of a lag deposit or an aeolian bedform).

Once all the data points sampling a soil target have been selected from the images, a quality check of the data acquired has been performed. Indeed, as the spectral quality can affect the quantification obtained, the quality of the spectra has been verified. To do so, only the spectra with a total signal emission higher than 1.10^{14} and with a signal-to-noise ratio higher than 1.10^{6} have been selected (only one data point was not meeting these criteria and was removed).

The last part of the data selection corresponds to the verification of any buried pebble. In Cousin et al. (2015), three different approaches were used to identify buried pebbles through shot-to-shot analyses: H signal, total signal variability, and ICA scores of Na and H. Clustered shot-to-shot data for the major elements and H signal were indicative of a buried pebble, along with a very stable shot-to-shot total intensity (as used in Hausrath et al., 2023). This method was difficult to use and Cousin et al. (2022b) have shown that the presence of some buried pebbles in the fine grained soil were not changing significantly the overall composition. Therefore, in this study, the most striking buried pebbles were identified by their shot-to-shot composition variation, mainly by looking at MgO vs SiO_2. Buried pebble detection using to the microphone shot-to-shot signal is in progress (Martin et al., 2023), and has not been used in this study. A total of 29 suspected buried grains were removed.

After selection, a total of 343 LIBS data points sampling a soil target are used in this study, corresponding to 46 different targets. There is no filter on distance on the selected data. 79% of them have been acquired at less than 4 m, 18% are between 4 m and 5 m, and only 3% were acquired over 5 m. The soil observations are located along the rover traverse in Fig. 1, and the list of the data points used in the study is shown in Table S1.

2.5. Grain size classification

Grain size classification of the 343 LIBS soil points has been performed using the RMI images. Some of these targets have also been observed by the Watson imager, and Vaughan et al. (2023) have quantified their grain sizes, their roundness as well as their colour distribution, for the entire field of view of each image. However here the objective is to investigate the grain size of the soil exactly where the laser hit the target. In that respect, the region of interest for the grain size analysis is localized around the LIBS spot only, and does not include the entire image. The SuperCam LIBS spot size is between 160–450 μm depending on the distance of the target (Maurice et al., 2021). Therefore, each point analysis encompasses a mixture of grains if these are smaller than the LIBS spot size.

Previous studies at Gale crater have used a very detailed grain size classification (Cousin et al., 2017b; Ehlmann et al., 2017), similar to the method described in Vaughan et al. (2023), where the roundness and colour of each grain is investigated. Concerning ChemCam analyses, the classification was very conservative, as all the detected buried pebbles were removed from the dataset (Cousin et al., 2015), or even the entire data point was also removed of the analysis (Cousin et al., 2017a).

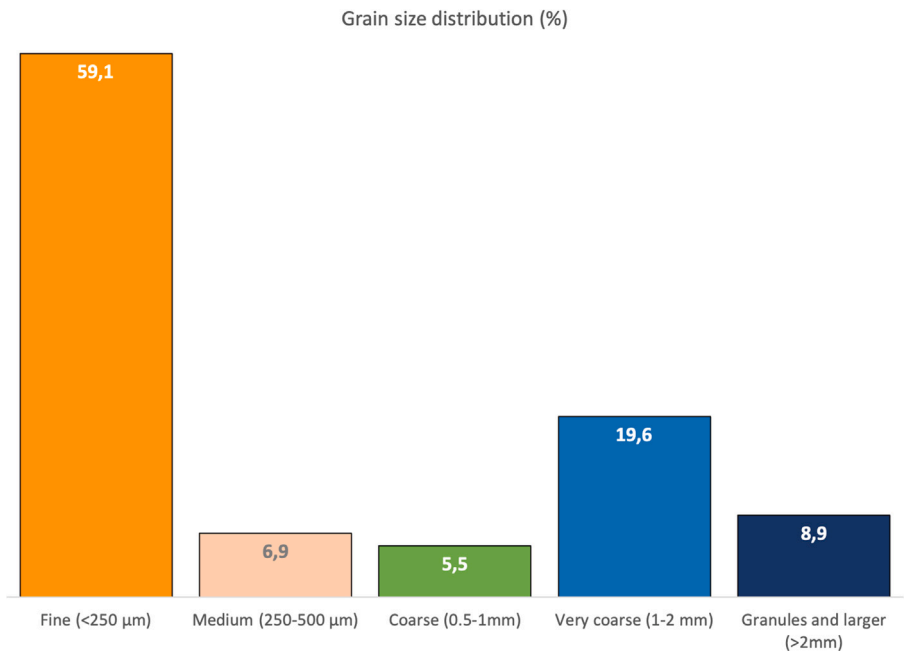

Fig. 2. Percentage of LIBS points for each grain size category.

However, Cousin et al. (2022a) have shown that these suspected buried pebbles were actually not affecting the average bulk composition of soil targets at Gale crater, as they shared the same composition of the fine-grained soil (only their shot-to-shot behaviour of the spectra intensity was different). Therefore, for this study, only a visual classification of the soil grain size around the LIBS spot has been performed, and the suspected buried pebbles have not been removed. Only the points with evident (from a change in chemistry) buried pebbles have been removed. In order to perform this grain size classification, the RMI before and after the LIBS activity are compared. It allows us to distinguish the grains that are present in the beam line before the LIBS shock wave moves them, and therefore assess to their grain size. This before/after LIBS RMI investigation is also necessary when looking for soil crust, as described in Hausrath et al. (2023). This methodology is used to classify each LIBS point analysis on a soil.

In the present study, RMI images have been investigated for each of the 46 soil targets analysed by SuperCam to classify each LIBS point on soil following the Wentworth scale (Wentworth, 1922), including fine-grained sand (<250 µm), medium sand (250–500 µm), coarse sand (0.5–1 mm), very coarse sand (1–2 mm), granule or larger gravel (>2 mm).

3. Results

3.1. Grain size classification

The visual grain size classification for each LIBS point shows that the vast majority of soil is fine grained (250 µm), representing 59% of the dataset (Fig. 2). Very coarse grains (1–2 mm) and larger (>2 mm) represent 29% of the dataset, whereas the medium (250–500 µm) and coarse (0.5–1 mm) grains correspond only to 12% of the data points. Therefore, this study will mainly focus on the chemistry and mineralogy of the very fine-grained and very coarse grained (and larger) soil targets.

As an example, the target called “Daa” was analysed on sol 357 (Fig. 3). This target is relatively heterogeneous in terms of grain sizes, as seen in Fig. 3A. Points 2 and 3 correspond to cobble gravels (around 1 cm), points 4 and 10 correspond to a very coarse sand (1–2 mm). All the other points have sampled a fine-grained soil (<250 µm). The LIBS craters are well observed (Fig. 3B), showing the non-cohesive aspect of the fine-grained soil.

The distribution of the analysed soil targets is not homogeneous along the traverse, as seen in Fig. 4. Indeed, most soil targets have been analysed in the Máaz formation and during the Delta Front campaign (Fig. 1). The Máaz formation represents an important igneous surface of the crater floor (Farley et al., 2022; Wiens et al., 2022; Udry et al., 2022; Liu et al., 2022; Sun et al., 2023) and therefore the rover spent a lot of time exploring this unit, which can explain why many soil targets were analysed there (around 240 sols were spent there). The majority of the soil targets analysed by SuperCam were observed during the Delta Front campaign, especially at Observation Mountain (the rover stayed at this location for 23 sols), at the base of the Jezero delta fan where the soil sample was collected by the sampling and caching subsystem (Hausrath et al., 2023). For a better understanding of the context where the soil samples have been acquired, many soil targets have been investigated there, including disturbed surfaces. Indeed, 25% of the fine-grained soil targets investigated by SuperCam are located at Observation Mountain. Seítah, an olivine cumulate (Farley et al., 2022; Wiens et al., 2022; Beyssac et al., 2023b), corresponds to the second geological formation investigated by Perseverance during the Crater Floor campaign (Fig. 1). However, the main focus was about the understanding of rock textures, chemistry and mineralogy compared to those observed at Máaz, and therefore fewer soil targets were analysed there.

3.2. Chemistry of the fine and very coarse-grained (and larger) soil

It is interesting to look at the chemistry of soil as a function of their grain size, in order to understand better their different sources, formation and/or alteration processes. Fig. 5 shows the chemical distribution for each major element for both fine-grained soil (<250 µm, in orange) and very-coarse grains and larger gravels (>1 mm, in blue) encountered all along the traverse up to sol 650. Several differences can be observed. The first one concerns the FeO and MgO contents. Coarser grains (in blue in Fig. 5) have a bimodal distribution for these two elements (mainly for MgO), leading to a higher average content. Actually, the bimodal distribution is observed for both fine and coarse-grained soil for the MgO content, even though it is more pronounced for the very

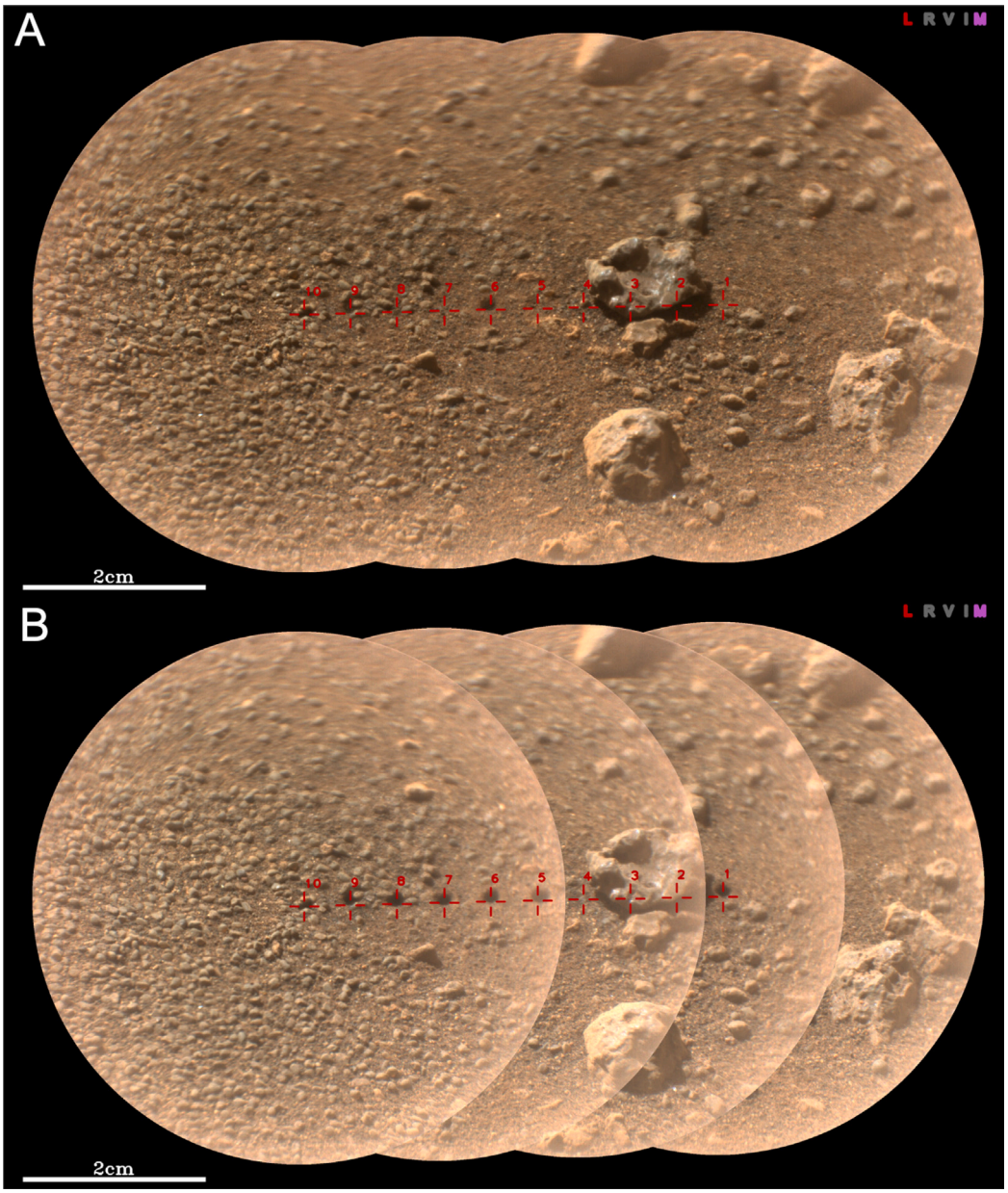

Fig. 3. RMI mosaic of the target called Daa using natural colours. A/ before LIBS, B/ after LIBS (LIBS pits visible in the fine-grained soil, i-e points 1 and 7). Credits: NASA/JPL-Caltech/LANL/CNES/CNRS.

coarse and larger grains. Moreover, very-coarse and larger grains show more extreme compositions for all the elements: a few points have a low content in SiO_2, and they show both lowest and highest TiO_2, Al_2O_3, CaO and Na_2O contents.

These different distributions can be observed in Fig. 6 as well. A clear mixing trend is observed for the very coarse and larger grains (>1 mm, in blue), between olivine, feldspar and clinopyroxene end-member (shown with a dashed line in Fig. 6), with a few shots trending towards the Fe–Mg apex and some others very close to the Si+Al apex. Shots trending towards almost pure feldspars explain the few data with the highest Na, K and Al contents in Fig. 5, along with the few shots towards Ca-rich pyroxenes that could be related to the Ca enrichment in a few shots. Nevertheless, the majority of the shots fall very close to the olivine end-member.

However, the fine-grained soil (in orange) shows much less dispersion. It shows a more pronounced trend between olivine and feldspar, with a vast majority of the shots falling in the middle of that trend, close to the dust signature (Lasue et al., 2023). No fine grains trend towards the Fe–Mg apex, and much fewer shots plot towards the clinopyroxene end-member compared to the very coarse grains, as expected from laboratory experiments (David et al., 2021).

The dispersion in composition is also well illustrated in the Daa target (Fig. 7). All the shots sampling a mixture of fine grains (shown as circles) fall into the middle of the mixing trend (Fig. 6/right), whereas the coarser grains (shown as crosses) plot either towards the olivine end-member (point 10) or towards the feldspar end-member (points 3 and 4).

Figs. 5 and 6 show that the fine-grained soil is overall homogeneous, with a composition of a mixture between basaltic and felsic components, with probably some dust. Some dispersion is still observed as some coarser buried grains can be still present in this dataset. On the other hand, the very coarse grains and larger gravels show a clear trend

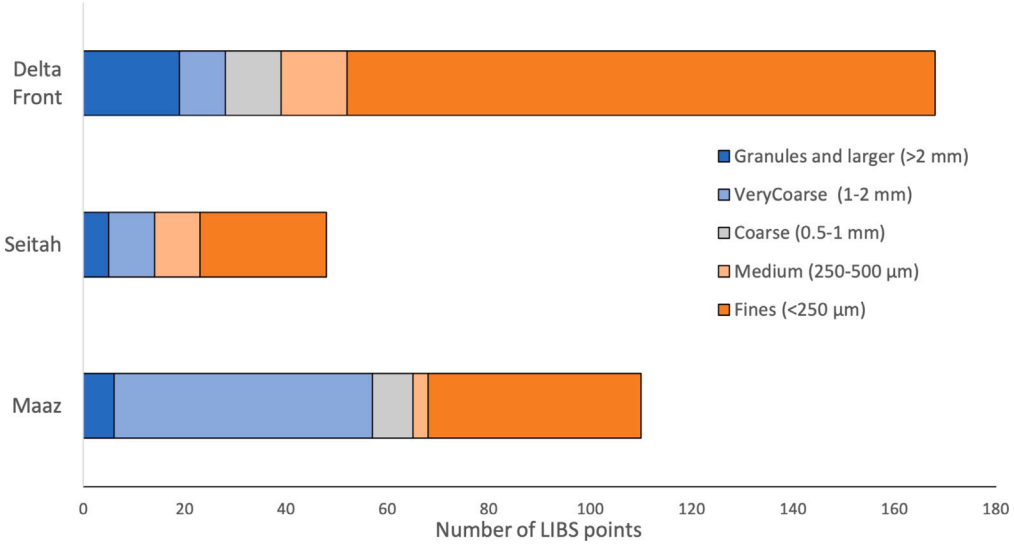

Fig. 4. Distribution of the LIBS analyses on the soil as a function of grain size and region of interest along Perseverance traverse.

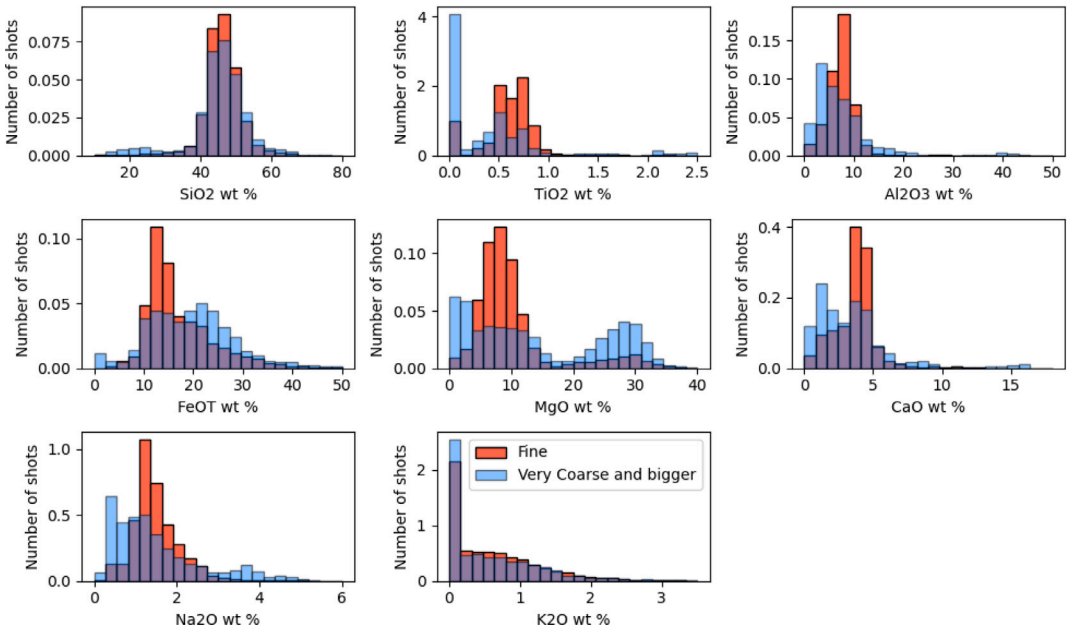

Fig. 5. Major element distribution of the shot-to-shot SuperCam data for the fine-grained (orange) and coarser-grained (very coarse and bigger - blue) soil. The first five shots have been removed, for each point, in order to remove the dust signature. Number of shots have been normalized for comparison. (For interpretation of the references to colour in this figure legend, the reader is referred to the web version of this article.)

between three main endmembers: olivine, feldspar and high-Ca pyroxenes - with however the majority of the data close to the olivine one.

The minor and trace element signatures in the fine-grained and coarser-grained soil have been investigated (Fig. 8). Coarser-grained (>1 mm) soil targets have higher signals in Mn, Li, and Ba, whereas fine-grained soil targets are more enriched in Sr. The Ni and Cr signals are very low in both datasets.

Even though the signal of H in LIBS data behaves differently between loose and consolidated targets (Rapin et al., 2017a,b), it has been demonstrated that it is a good indicator of hydration in granular materials such as soil targets, independently of the grain size (David et al., 2021). Both fine grains and very coarse grains contain some volatile elements such as Cl, H and S. Fine grains observed at Jezero are clearly more hydrated compared to the coarser grains (Fig. 9). However, some of the coarse grains show a H signal similar to that of the fine grains, and this seems consistent with the fact that some alteration rinds have been detected in some of the coarser grains (Hausrath et al., 2023). Cl is difficult to observe and most of the data do not show any line for this element. However, fine-grained soil is slightly more enriched in Cl compared to the larger grains (Fig. 9). The sulfur signal is also higher in fine-grained soil. Volatile elements do not show any obvious correlation with major elements (See Figures S1, S2 and S3 in Supp. Material). However, these elements are correlated with each other (Fig. 10), mainly H and S that have a R^2 of 0.93.

Looking at the composition of soil at the different locations of the rover in the crater floor (up to sol 650 - Fig. 1) could help investigate the different possible sources for the coarser grains, as well as the size threshold for their transport. Concerning the fine-grained soil, the vast majority of the data overlap in the middle of the trend from basaltic to more felsic (Fig. 6/right) and the same is observed for the four regions where most of the fine-grained material has been analysed (Màaz, Séítah, Observation Mountain and the rest of delta front - Fig. 11).

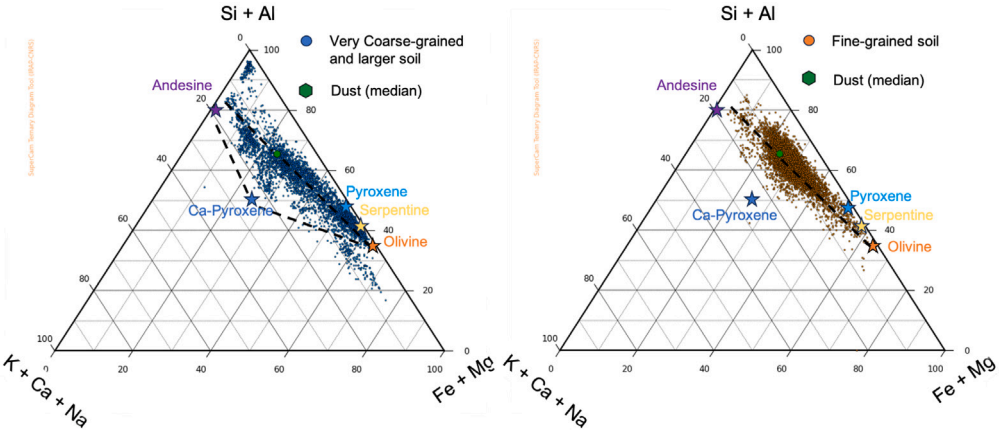

Fig. 6. Ternary diagram (molar Si+Al/K+Ca+Na/Fe+Mg) for the very coarse and larger grains (>1 mm, left, in blue) and for the fine-grained soil (<250 μm, right, in orange) observed by SuperCam. All the shots (except the first 5) are displayed. The ideal compositions of the calibration targets are shown in different symbols for Ref. Cousin et al. (2022c) and dashed lines represent the main trends. The median composition of the dust is shown as well Lasue et al. (2023). (For interpretation of the references to colour in this figure legend, the reader is referred to the web version of this article.)

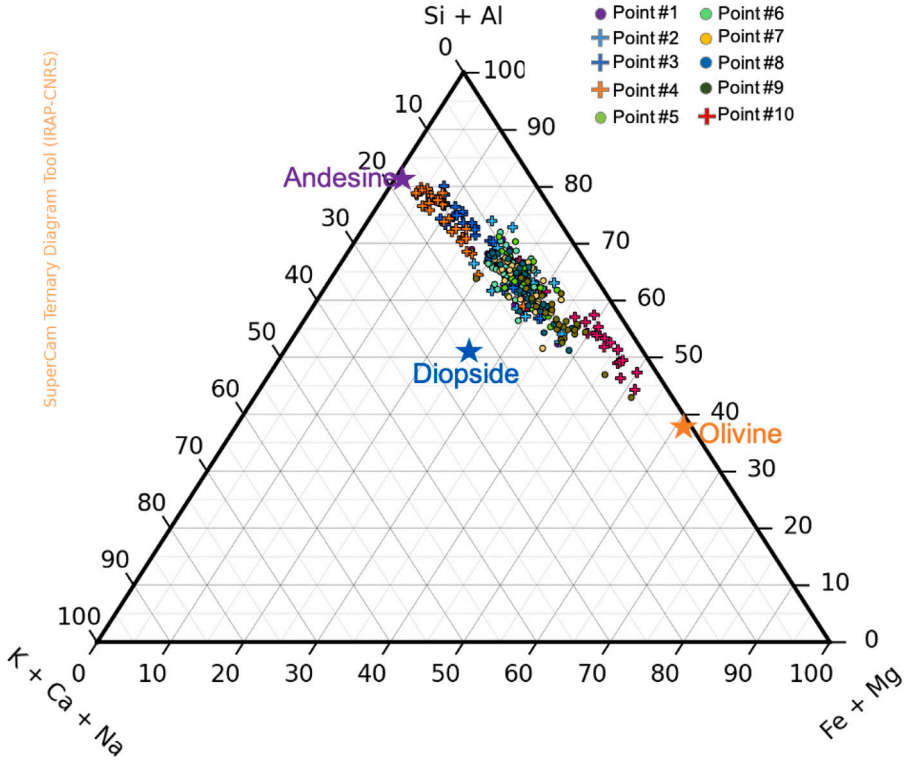

Fig. 7. Ternary diagram (molar Si+Al/K+Ca+Na/Fe+Mg) for the Daa target. Each data point is represented in a different colour and each shot is presented (after shot #5 to remove the dust contribution). Points 2, 3, 4 and 10 have a different symbol, as those points correspond to very coarse grains or larger gravels, whereas the other points are fine grains.

Fig. 12 shows that the coarser grains have a larger dispersion in the Máaz formation, probably because the dataset is larger. Very coarse grains observed in Observation Mountain represent two main types of compositions: some grains correspond to a mixture of different phases (similar to the fine-grained soil), and some trend towards the Fe+Mg apex. At Séítah, the same two populations are observed, but with also a lot of shots very close to the olivine end-member. Data from the delta front are overall similar to the previous regions. However, no shots trend towards the Fe+Mg apex whereas some plot very close to the Si+Al apex.

These observations show that the chemistry of fine-grained soil is similar to each other all along the traverse. The very coarse grained soil show pretty much always the same variability along the traverse, with chemistry generally close to olivine, or some mixtures of different phases. However, there seems to be a relation with the location of the rover, with more outliers (Si–Al rich) in the delta front regions.

3.3. Mineralogy of the fine and very coarse-grained (and larger) soil

The mineralogical composition for this study can be assessed via SuperCam through the LIBS technique (ternary diagrams will give some hints, and stoichiometry when possible) and through the VISIR data.

3.3.1. Mineralogical assessment from LIBS

Some distinct mineralogies can be assessed via stoichiometric analyses from the LIBS data, as explained in the methodology section and

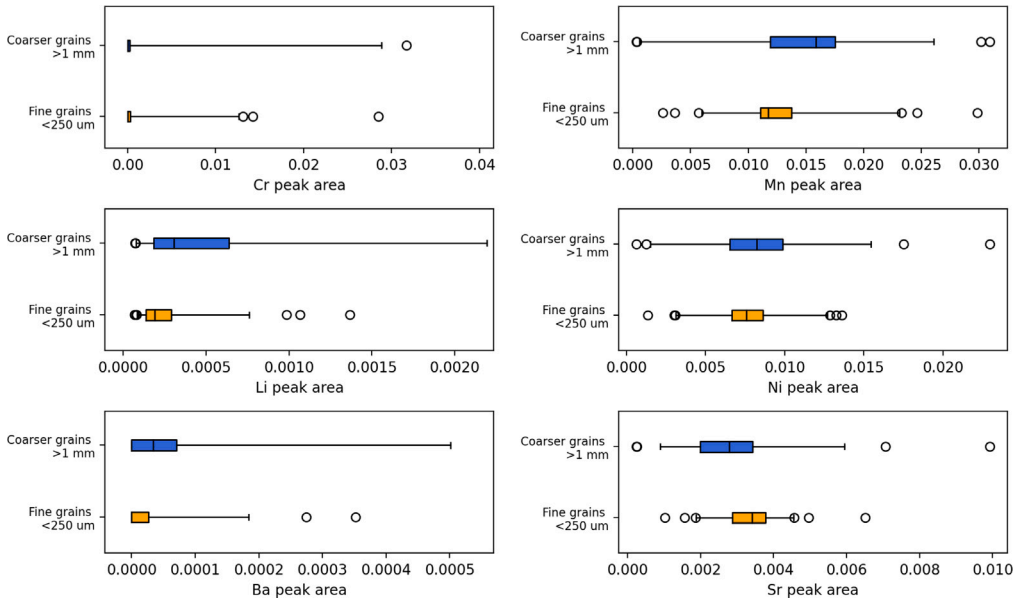

Fig. 8. Boxplot distribution of the main minor and trace elements observed in LIBS spectra. The rectangle shape corresponds to the first and third quartiles. The median is shown as a line in that rectangle. Outliers are shown as circles.

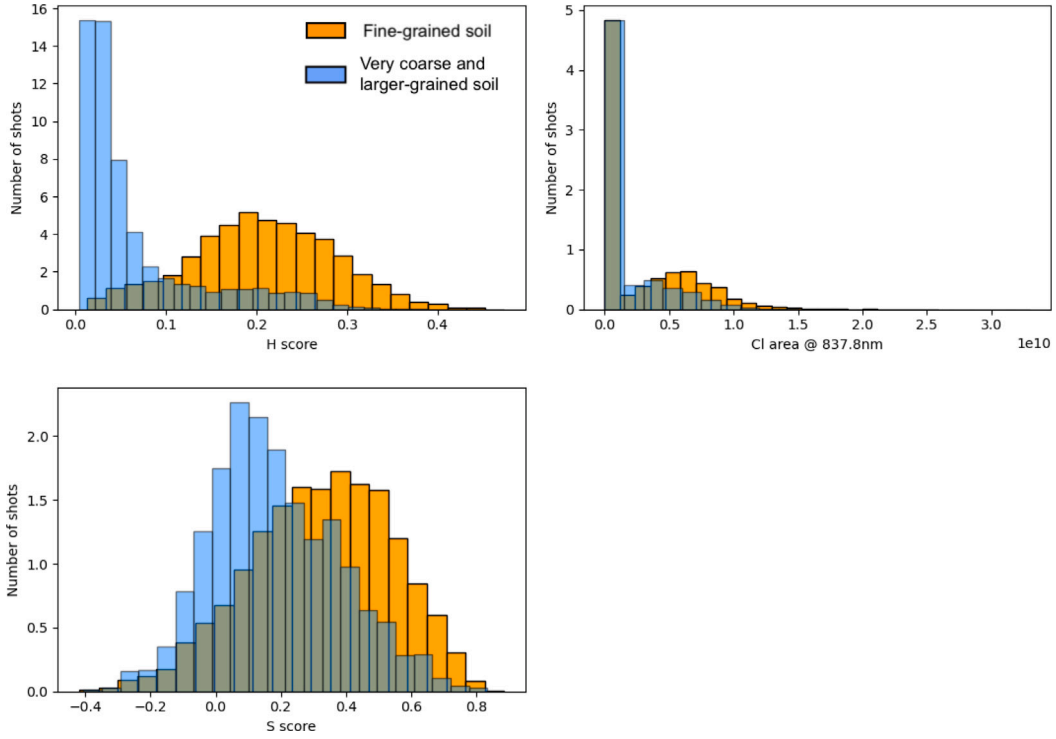

Fig. 9. Distribution of the H, Cl and S signatures in both fine-grained soil (<250 μm, orange) and larger-grained soil (>1 mm, blue) in Jezero's soil. The data are normalized in order to compare them, as the number of points between the fine-grained and the very coarse and larger grains is different. (For interpretation of the references to colour in this figure legend, the reader is referred to the web version of this article.)

from Beyssac et al. (2023a) and Udry et al. (2022). We have not identified any point with a composition consistent with pure plagioclase in the soil targets, although some points locally approach a plagioclase composition (Fig. 6). Among all the soil targets, we identified 19 and 5 points having a composition consistent with pure olivine and pyroxene, respectively. Note that our criteria are highly restrictive and that many other points have compositions really close to pure olivine and pyroxene.

Olivine grains are found on the crater floor as well as on the delta front not far from the sampling location, only in coarse-grained soil (seven of them actually correspond to buried coarse grains). Fig. 13 shows that these olivine grains have Fo# (where Fo# is the molar Fe/(Fe+Mg)x100) in the range 52–69 matching well the range of olivine Fo# in the Séítah unit (Beyssac et al., 2023a).

Pyroxene grains were mostly detected on the crater floor and only one point was detected in the delta front. Pyroxene grains are found mainly in very coarse-grained soil (only one has been found in a fine-grained soil). Pyroxene grains include low Ca orthopyroxene and pigeonite ($Wo_{3\text{-}14}Fs_{42\text{-}78}En_{19\text{-}51}$) as well as high Ca diopside ($Wo_{41\text{-}44}Fs_{18\text{-}33}En_{23\text{-}41}$) compositions. Wiens et al. (2022) noted that

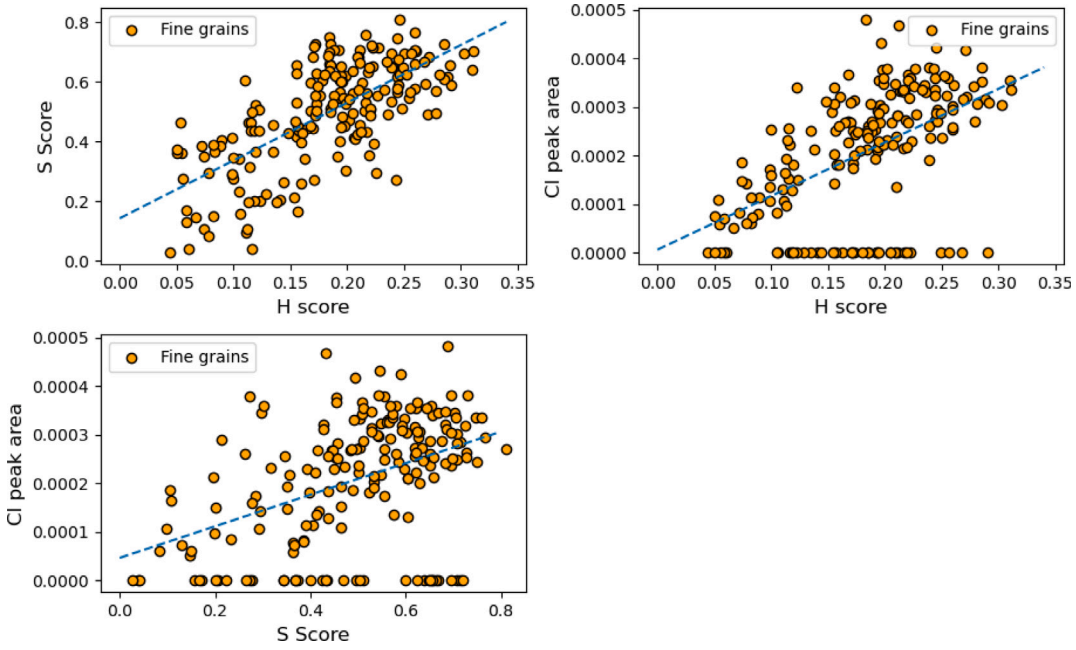

Fig. 10. Point-to-point Cl peak area, H and S scores for fine-grained soil at Jezero. Blue dashed line corresponds to a linear fit, including the data points where Cl peak areas is 0.

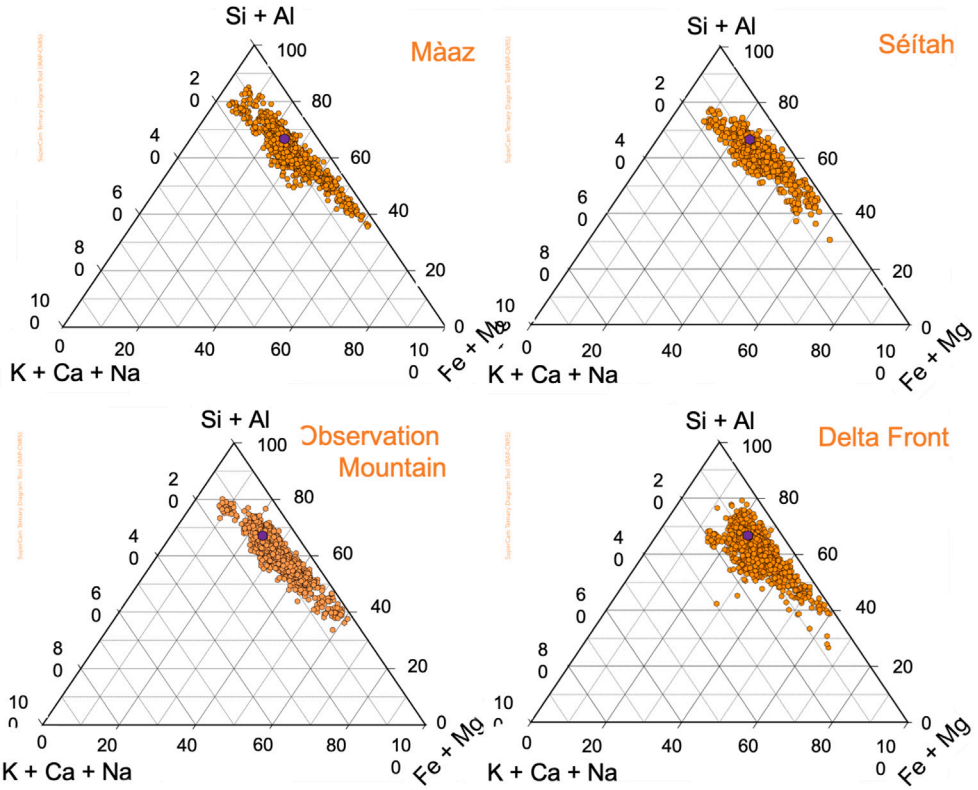

Fig. 11. Ternary diagram (molar Si+Al/K+Ca+Na/Fe+Mg) for fine-grained soil at each region of the traverse. Technically Observation Mountain is in the Delta Front, but is shown on its own as it is the soil sampling location. All the shots (except the first 5) are shown. Median composition of the dust is shown in purple for comparison (Lasue et al., 2023). (For interpretation of the references to colour in this figure legend, the reader is referred to the web version of this article.)

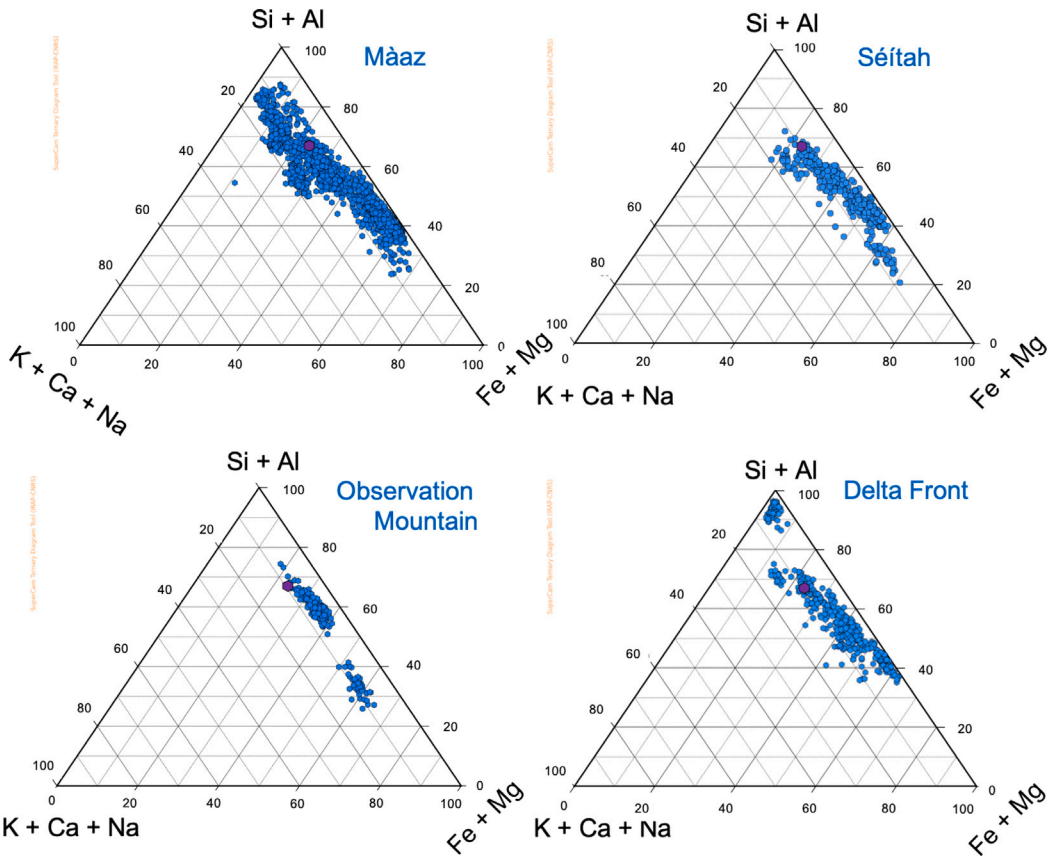

Fig. 12. Ternary diagram (molar Si+Al/K+Ca+Na/Fe+Mg) for very coarse-grained soil at each region of the traverse. Technically Observation Mountain is in the Delta Front, but is shown on its own as it is the soil sampling location. All the shots (except the first 5) are shown. Median composition of the dust is shown in purple for comparison (Lasue et al., 2023).

Artuby ridge, bounding the explored portion of Séítah on the southwest side, was especially rich in high-Ca pyroxene. Fig. 13 shows the compositions of the pyroxene grains compared to the pyroxene composition in the Séítah (Beyssac et al., 2023a) and Máaz (Udry et al., 2022) units. For low and high Ca pyroxenes, some grains have compositions matching the compositions observed in Séítah while some other grains match the Fe-rich compositions observed in Máaz. This suggests that the pyroxene grains in the soil have inputs from these two formations.

Some very coarse grains seem to have a particular mineralogy, different from primary minerals. From the ternary diagram, some shots are particularly enriched in Fe and/or Mg and trend towards the Fe+Mg apex (Fig. 6a). These correspond mainly to AEGIS_0456B point 2, as well as Granite_Peak pt 9. Granite_Peak point 9 has a low total of oxides (average at 67.3 wt%), and a low SiO_2 content (<21wt%) whereas its FeO content is quite elevated (average at 25.6 wt%). MgO is slightly elevated, to a lower extent (average at 13.6 wt%). There is however no clear trend between the SiO_2 content and FeO nor with MgO, all of these being relatively stable shot to shot. This point has a C/O signal similar to previous carbonates that have been detected along the traverse (Clavé et al., 2022), which therefore favours the Fe/Mg-carbonate hypothesis.

Similarly, Aegis_0456B point 2 does not show any trend between $SiO_2$and FeO or MgO. The SiO_2 content is low (18.2 wt% in average), with an elevated FeO and MgO content (25.8 wt% and 31.2 wt% in average, resp.). The sum of oxides (considering the major elements only) is however higher than that of Granite_Peak pt 9, at 85.7 wt% in average. The shot-to-shot content is very stable for FeO, MgO and SiO_2. This point also seems to be enriched in carbonate, from the C/O analysis (Clavé et al., 2022).

Some other particular shots from the very coarse grained soil (Fig. 6a) show a very distinct composition, very close to the Si+Al apex: "Gas_Creek" (pt 6) is really enriched in SiO_2 (74wt%) whereas the target "Barrier_Range" (pt 5) is enriched in Al_2O_3 with more than 40 wt%. Al-rich targets have been observed along the traverse, presenting diverse textures and mineralogical compositions. Barrier_Range corresponds to a smooth light-toned pebble that presents a low hydration, with a signature corresponding to a mixture with different phases, including kaolinite. Such Al-rich targets are discussed in specific papers (Royer et al., 2024; Forni et al., 2024).

3.3.2. *Mineralogical assessment from VISIR*

VISIR data can also be used to investigate mineralogical differences between the fine-grained and the very coarse-grained (and larger) soil targets (Fig. 14). Some coarse-grained soil points show a strong 1.3–1.8 μm slope, which corresponds to the longward side of a broad $Fe2^{2+}$-related absorption band typical of an olivine spectrum (King and Ridley, 1987; Viviano et al., 2014; Mandon et al., 2020; Royer et al., 2020). This is consistent with the overall LIBS chemistry showing most of the coarse grains close to the olivine end-member in ternary diagrams. The highest VISIR slope corresponds to the points identified as olivine by stoichiometric analyses (targets Hastaa pts 1, 10 and Gas_Creek pt 8 for example), along with other points. Olivine has also been detected with LIBS in many rocks from the crater floor (Beyssac et al., 2023a; Liu et al., 2022; Wiens et al., 2022) and the delta (Beyssac et al., 2023b; Dehouck et al., 2023). The 1.3–1.8 μm slope in fine-grained soil is homogeneous and flatter (Fig. 15). Besides the olivine signature, some coarse grains seem to be more hydrated, with a deeper 2.3 μm band as well. These points correspond to Granite_Peak target (mainly point

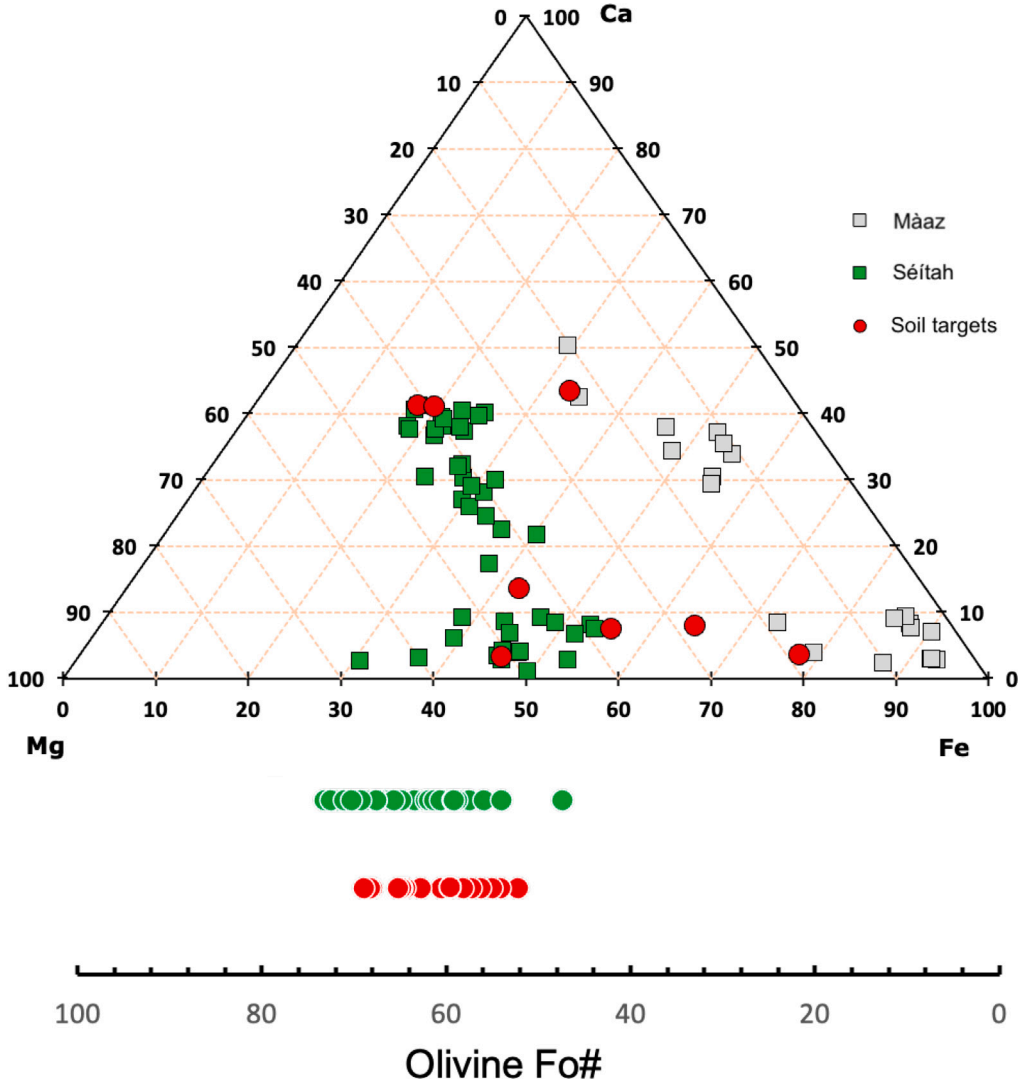

Fig. 13. Pyroxene and olivine composition observed in bedrock from Séítah and Màaz units (green squares) compared to those found in very coarse and larger-grained soil targets (red circles). The olivine and pyroxene compositions are only found in soil where the grain is large enough (compared to the laser sot size) to represent a pure mineral composition, and this is why these observations are relatively rare. (For interpretation of the references to colour in this figure legend, the reader is referred to the web version of this article.)

4) and Gas_Creek (point 2), and this signature could be attributed to the presence of phyllosilicates. Only one point (Red_Mountain point 1, from the Delta Front) shows some carbonate signature, showing a deeper 2.3 and 2.5 μm absorption band. Granite_Peak pt 9, found to be a carbonate from the LIBS analysis, does not particularly shows up in Fig. 14, probably due to the different field of view between the different techniques.

On the other hand, the fine-grained soil shows overall less dispersion. It seems to have a greater proportions of ferric oxides/oxyhydroxides, as the band depth at 545 nm is more pronounced. These ferric oxides/oxyhydroxides could correspond to small particles, as no pure Fe oxide has been observed with the LIBS technique in the fine-grained soil (Figure S4 in Supp. Material). Also, the finest soil targets tend to have a stronger absorption for the low-Ca pyroxenes (and maybe for the pyroxenes in general). Interestingly, from the VISIR data, the fine-grained soil is not particularly hydrated compared to the coarser-grained, and lack absorptions related to carbonates and phyllosilicates. This VISIR signature seems consistent with the fact that no particular mineralogy has been detected with LIBS stoichiometry, confirming some fine-grained mixtures of different phases or compositional control by a variable-composition amorphous phase such as glass (Rampe et al., 2020).

4. Discussion

4.1. Grain size

Our grain size classification shows that the soil targets analysed by SuperCam are mostly made of fine-grained components (<250 μm, representing 59% of the data points) followed by very coarse and larger components (>1 mm, representing 29% of the dataset). Medium and coarse soil components (between 250 μm and 1 mm) represent a minority, only 12% of the dataset. This grain size distribution, showing a lack of grains between 250 μm - 1 mm was observed already during the MER missions (Sullivan et al., 2010). In fact, moderate-size grains below 900 μm are thought to be relatively short-lived (Sagan et al., 1977), as their size makes them more prone to saltation. Due to high kinetic collisions they suffer greater attrition, with a relatively rapid reduction in grain size (Sullivan et al., 2010; Hausrath et al., 2023), explaining their rarity in martian soil.

4.2. Very coarse-grained (and larger) soil

Stoichiometric analyses of the SuperCam LIBS, along with VISIR observations have shown some specific mineralogies among the very

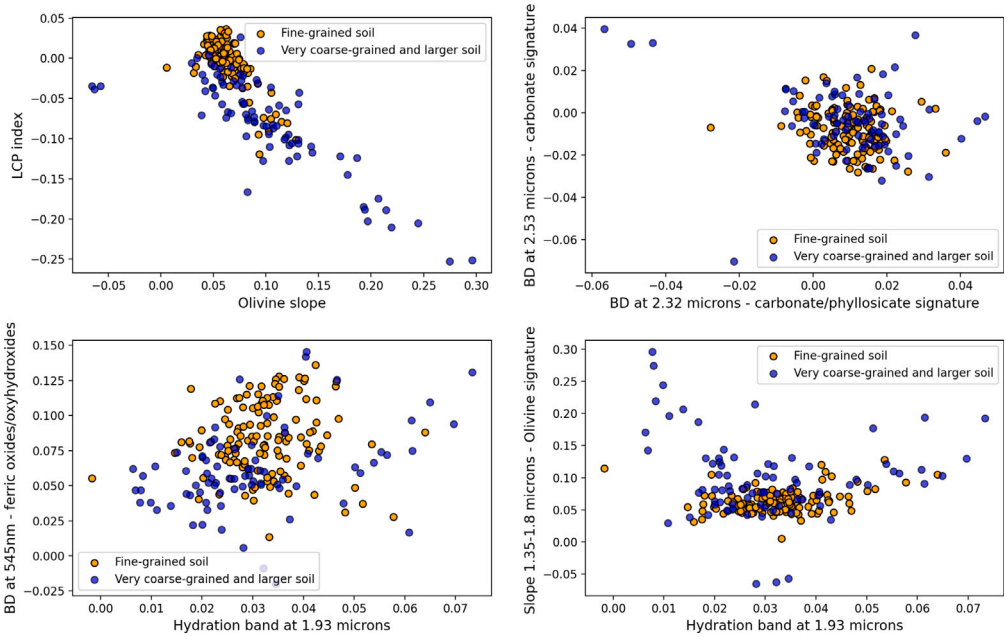

Fig. 14. VISIR spectral parameters for the fine-grained and coarser-grained and larger soil targets. LCP index is from the band depth at 1.86 μm and the olivine slope is the slope from 1.35 and 1.8 μm. BD stands for "Band Depth". (For interpretation of the references to colour in this figure legend, the reader is referred to the web version of this article.)

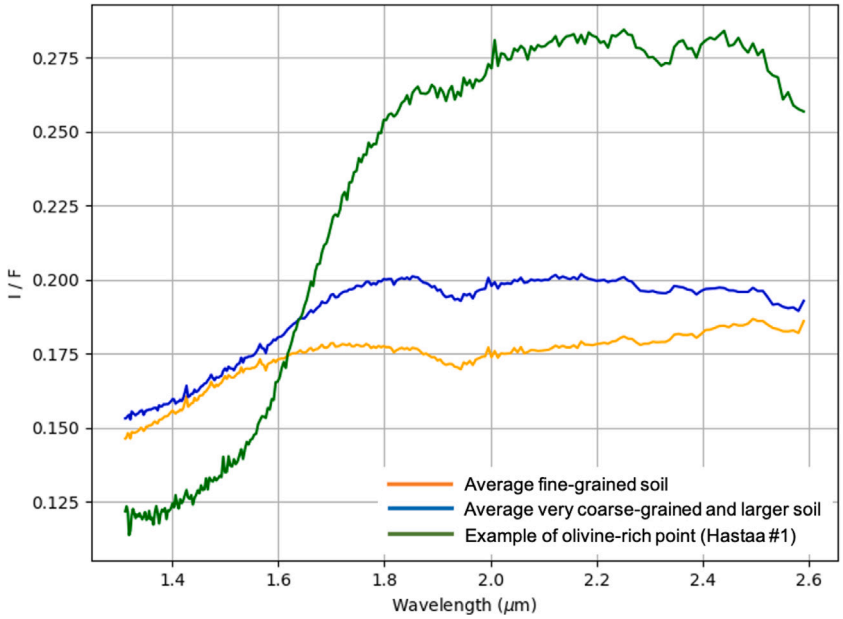

Fig. 15. IR average spectrum of fine-grained soil (orange) and of very coarse-grained (and larger) soil (in blue). The green spectrum corresponds to Hastaa pt 1, which is an olivine-rich pebble, as identified by LIBS as well. (For interpretation of the references to colour in this figure legend, the reader is referred to the web version of this article.)

coarse and larger soil targets (>1 mm grain size) analysed at Jezero, such as olivine (19 points), pyroxenes (5 points), phyllosilicate-rich (2 points) and carbonate-rich (3 points) ones. These mineralogies are consistent with the analyses performed by WATSON and PIXL (Bhartia et al., 2021; Allwood et al., 2020) at the soil sampling location (one disturbed target, "Topographers Peak", and one undisturbed, "Marmot Bay", at Observation Mountain) (Hausrath et al., 2023).

In-situ investigation of Jezero has revealed that the crater floor bedrock is enriched in mafic minerals such as pyroxenes and olivines (Udry et al., 2022; Wiens et al., 2022; Farley et al., 2022; Liu et al., 2022). Even though the Máaz formation contains principally Fe-rich pyroxenes (Udry et al., 2022), the Séítah formation is particularly enriched in phenocrysts of olivines (Mg# between 0.55 and 0.74) that are relatively pristine, this formation being interpreted as a cumulate (Beyssac et al., 2023a; Liu et al., 2022). Therefore, olivines and pyroxenes found as very coarse and larger soil grains can come from the erosion of local rocks, as suggested for the olivine-rich pebbles found in the Máaz formation in Beyssac et al. (2023b), Hausrath et al. (2023), Vaughan et al. (2023) and Mandon et al. (2023).

A specific mineralogical composition other than primary igneous is found in several coarse-grained soil targets from the Delta Front campaign. Some points from the Granite_Peak target at Observation Mountains present the deepest band at 2.32 μm in the VISIR data (Fig. 14). Another coarse grained soil target, located at Enchanted Lake (called Gas_Creek pt 2) in the Delta Front investigation, shows a similar phyllosilicate signature. Moreover, a carbonate signature has

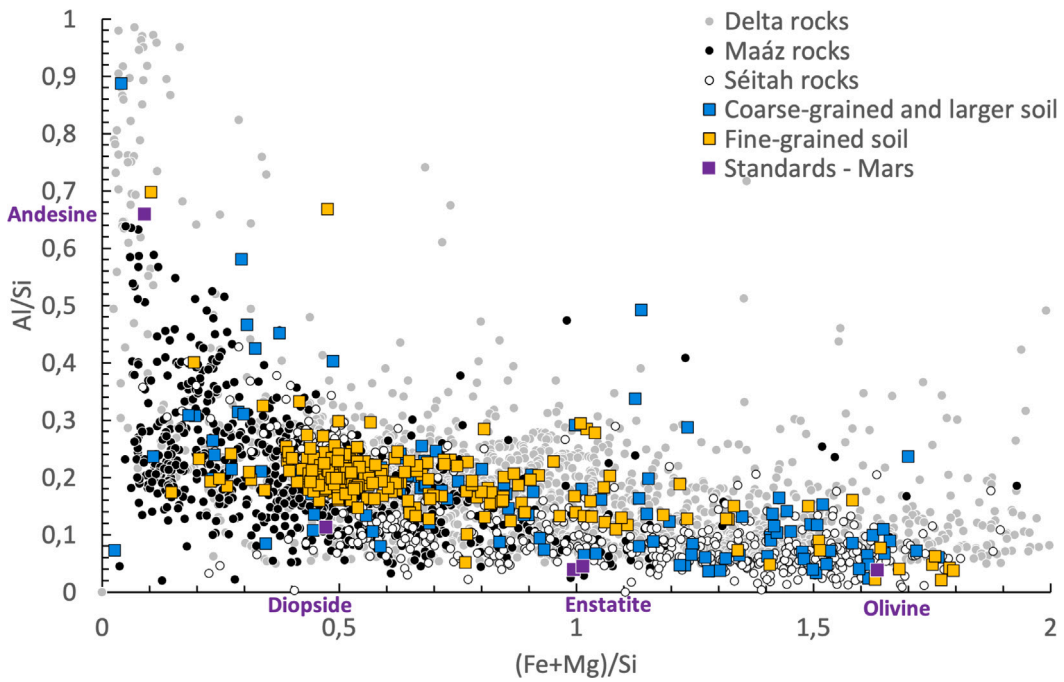

Fig. 16. Al/Si vs (Fe+Mg)/Si (molar) for the fine and very coarse-grained soil (and larger). Bedrock observed in Máaz, Séítah and Delta are shown for comparison. Reference standards are shown in purple. (For interpretation of the references to colour in this figure legend, the reader is referred to the web version of this article.)

been observed in one coarse-grained soil target (Red_Mountain pt 1), also located in the Delta Front area (Cannery Passage). These carbonate and phyllosilicate signatures in soil targets have only been observed in the very coarse-grained soil, in the vicinity of the Delta Front. Delta Front bedrock has been shown to significantly contain more secondary phases compared to the crater floor bedrock (Dehouck et al., 2023; Hausrath et al., 2023). These observations are consistent with the presence of carbonate and/or phyllosilicate-rich coarse grained soil coming from local bedrock of the Delta Front. Discussions about the different hypotheses for the formation of such secondary materials in the Delta Front are still ongoing, even though the presence of phillosilicates indicates a low temperature alteration (Dehouck et al., 2023).

There are no other clear detections of possible alteration phases in the coarse-grained material elsewhere in the soil of the crater floor, which is also consistent with the low alteration of the crater rock bedrock (Udry et al., 2022; Mandon et al., 2023; Wiens et al., 2022; Farley et al., 2022).

The chemistry of the soil has been compared to that of the various bedrock analysed by SuperCam in the Máaz, Séítah, the Delta Front and Delta Top areas. These bedrock show distinct chemical and mineralogical compositions due to different formation processes and sources, as discussed in several previous studies (Wiens et al., 2021; Beyssac et al., 2023a; Udry et al., 2022; Dehouck et al., 2023; Mandon et al., 2020). Even though the soil targets show some overlap, as seen in Figs. 5 and 6, the very coarse and larger soil data (in blue) mainly plot close to the olivine standard (around (Fe+Mg)/Si =1.6), thus overlapping with the rocks observed in Séítah. This is consistent with the hypothesis of a local contamination from these rocks, as discussed in more details in Beyssac et al. (2023b). The rocks observed in the delta show a wide range of compositions and there is no evidence of relationship between those and the soil observed in the crater floor.

Very coarse-grained and larger soil (>1 mm) observed at Jezero has a very different composition from those observed at Gale crater. Very coarse grains and pebbles encountered in the soil at Gale crater have indeed a felsic composition (Meslin et al., 2013; Cousin et al., 2015, 2017b; O'Connell-Cooper et al., 2017; Ehlmann et al., 2017). This was interpreted as a local contamination from the erosion of felsic float rocks that were encountered mainly at the beginning of Curiosity's traverse (Cousin et al., 2015; Sautter et al., 2015; Payré et al., 2020), as these felsic pebbles were observed in the same area (Cousin et al., 2015).

4.3. Fine-grained soil

We have shown that Jezero fine-grained soil targets have overall a similar composition all along the traverse inside the crater floor of Jezero, very close to the dust signature. However some contamination from local bedrock or local pebbles has been observed via the enrichment in Mg in some shots. Moreover, a few shots from the delta Front location (at Cannery_Passage and Three Forks) deviate towards the Al+Si apex in Fig. 11. These few Al-rich shots could be explained by a local contamination from the erosion of local Al-rich rocks observed at this location (Royer et al., 2024; Forni et al., 2024), as also suggested in Fig. 16.

Mineralogy of the fine-grained soil is difficult to assess using the LIBS technique, as a new mixture of grains is sampled by each laser shot. Laboratory experiments in granular media showed that only the surface (to around 1 μm depth) of the grains is measured with LIBS when the grain size is <500 μm, and that for mechanical mixtures the end-member compositions can be retrieved depending on the grain size of the mixture (David et al., 2021). Concerning Jezero fine-grained soil, Fig. 6b shows that its composition is very similar to that of dust (Lasue et al., 2023). From this mixing line between feldspars and mafic minerals, we can estimate the proportion between the two end-members at around 47% feldspars and 53% mafic minerals. This fine-grained soil is more enriched in mafic minerals compared to the dust, and this has be attributed to some local contamination.

PIXL and SHERLOC data acquired at Observation Mountain have shown that the fine-grained soil was consistent with mainly primary phases, with a few signatures of Mg-sulfates, carbonates and Cr–Ti–Fe oxides (Hausrath et al., 2023). With SuperCam, only a few (<10) shots trending towards Fe oxides were observed (Figure S4 in Supp. Material). In addition to the fact that all these secondary-phase grains are small (<150 μm) and mixed together, they represent a small volume of the fine-grained soil, and this can explain why they have not been detected in the fine-grained soil with SuperCam. SuperCam's Cl, H and S

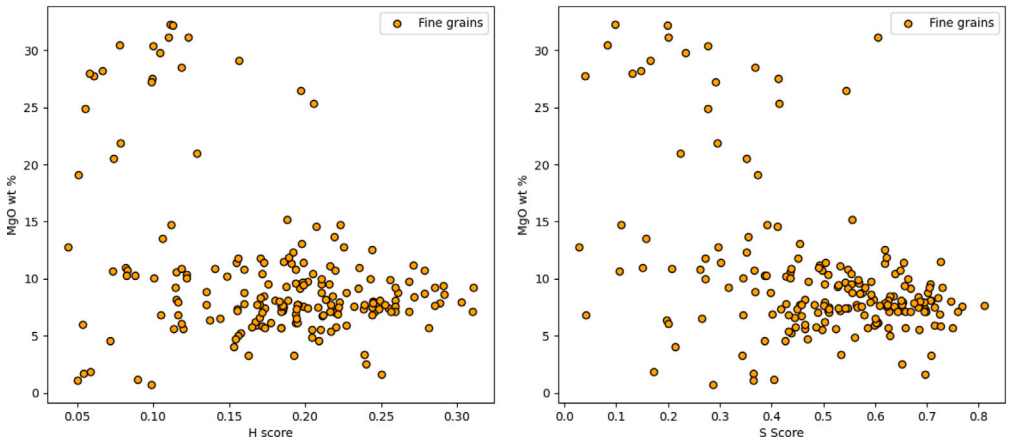

Fig. 17. MgO (wt%) vs H score (left) and MgO (wt%) vs S score (right) for the fine-grained soil. This figure shows only the point-to-point data instead of the shot-to-shot data, as the S score cannot be determined for shot-to-shot data in soil.

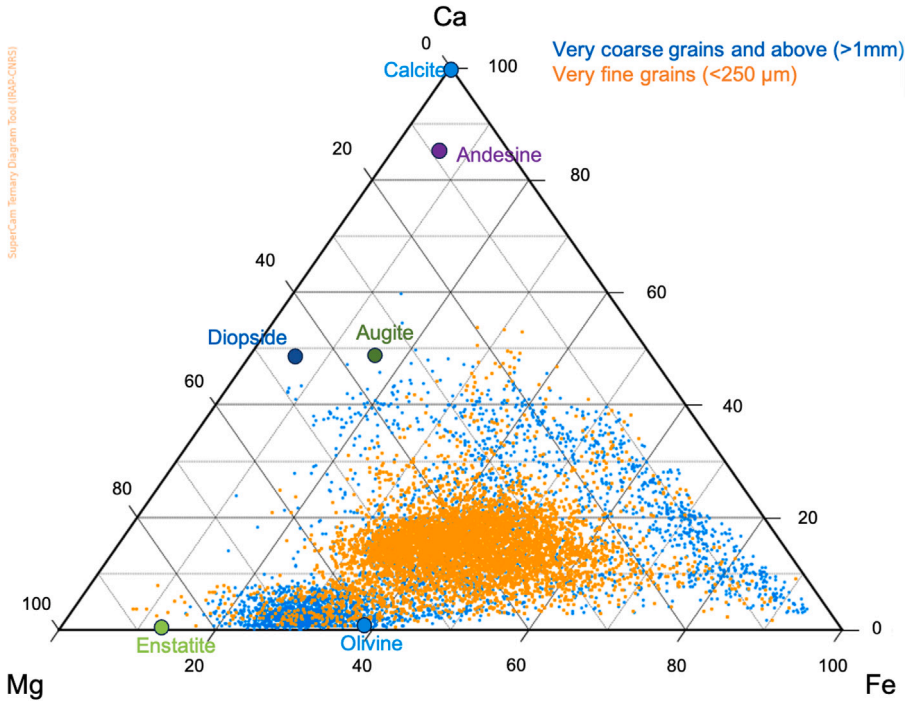

Fig. 18. Ca-Fe–Mg ternary diagram for very coarse grains (blue) and very fine-grained (orange) soil at Jezero. SuperCam calibration targets are shown in circle for reference. (For interpretation of the references to colour in this figure legend, the reader is referred to the web version of this article.)

signals are higher in fine-grained soil compared to coarser grained soil, but no obvious signatures of Mg-sulfates or carbonates were detected (Fig. 17).

Fine-grained soil targets analysed by SuperCam all along the traverse do not show any clear VISIR signature (Fig. 15), which is surprising compared to other studies (Vaughan et al., 2023; Hausrath et al., 2023; Mandon et al., 2023).

Nevertheless, the LIBS shot-to-shot technique clearly shows a mixture of primary phases in the ternary diagrams and Harker plots (Figs. 11 and 16). The Ca-Mg-Fe ternary diagram (Fig. 18), shows that the fine-grained soil (in orange) has only a few shots trending towards specific end-members. The coarser grains shown in blue in Fig. 18 are clearly dominated by olivine, high- and low-calcium pyroxenes, as expected from laboratory LIBS experiments on granular medium (David et al., 2021). These observations are also consistent with the stoichiometric analyses presented in Section 3.3.1, and with the fact that this component is made of a mixture of primary phases, with no distinction.

Moreover, the Chemin instrument at Gale crater showed that the fine-grained soil is made of 35 +/− 15 wt % XRD amorphous component, along with > 60 wt % primary minerals and a small amount of secondary phases. When taking into account the mineral abundances renormalized to 100% crystalline phase, the main constituents correspond to plagioclase (40.8 wt% plagioclase, 28 wt% pyroxenes, 22.4 wt% olivine) (Blake et al., 2013; Rampe et al., 2018). From our analysis, Jezero fine-grained soil presents a similar mineral mixture to Gale's fine-grained soil, with slightly more mafic minerals compared to the feldspars, almost in equal mixture.

Jezero crater fine-grained soil is more hydrated compared to the coarser grains (>1 mm) soil (Fig. 9). However, our preliminary analysis does not show any evidence of hydrated Mg-sulfates, even though some presence of sulfate has been detected at the soil sampling location by SHERLOC (Hausrath et al., 2023) and elsewhere in crater floor and delta bedrock (Phua et al., 2023), and also by SuperCam in some crater-floor bedrock (Meslin et al., 2022). On the other hand, the H

signal correlates to Cl and S. This correlation has been attributed, at least partially, to the presence of soil crust that is enriched in salts such as perchlorates and sulfates (Hausrath et al., 2023). Moreover, some salts such as perchlorates have been detected in some crater floor bedrock (Meslin et al., 2022; Wiens et al., 2022), but also at different landing sites in soil (especially perchlorates) (Clark, 1993; Arvidson et al., 2011; Kounaves et al., 2014). Besides with Cl and S, H signal does not correlate with any other element, even major ones (see Figures S2–S4 in Supp. Material). Therefore, the observed hydration does not seem to be particularly related to the presence of carbonates or phyllosilicates, which is consistent with SHERLOC's observations (Hausrath et al., 2023).

Contrary to the LIBS observations, the VISIR signature of the fine-grained soil (Figs. 14 and 15) does not show any clear evidence of hydration. Indeed, the 1.9 μm absorption band is relatively small, as presented also in Hausrath et al. (2023) and Vaughan et al. (2023). Moreover, the 1.9 μm band is less distinct in fine-grained soil compared to rocks from the crater floor (Mandon et al., 2023), which is the opposite of what is observed with LIBS data. This lack of hydration signature in the VISIR data of the fine-grained soil can be explained by several factors. First, hydrated phases are small by definition in our classification < 250 μm and are potentially aerosols of micron size. In this size regime, absorption bands in the VISIR spectrum are diminished if not absent (Pommerol and Schmitt, 2008b,a; Sultana et al., 2021), which can explain the overall lack of signature in the VISIR data. Therefore, if hydration comes from very fine-grained components (as observed from Gale crater data Rampe et al., 2018; Blake et al., 2013; Ehlmann et al., 2017; Cousin et al., 2017b), it would be difficult to identify it with VISIR. The presence of Fe oxides can make the detection even more complex and such phases have been detected from PIXL (Hausrath et al., 2023).

Secondly, the main hydration band observed by SuperCam is located at 1.9 μm, as the SuperCam IRS range goes up to 2.6 μm. Besides its dependency to grain size (Pommerol and Schmitt, 2008b,a), this absorption band is mainly related to structural or molecular water. We do not have access to the 3 μm absorption band that is mainly related to adsorbed water (Pommerol et al., 2009). Therefore, if the water in the soil is present in the form of adsorbed water, then the 1.9 μm band will not necessarily be significant, as shown in Pommerol et al. (2009). Adsorbed water in fine-grained soil has been observed already with previous missions, such as at Gale crater via the SAM instrument (Leshin et al., 2013; Ehlmann et al., 2017). Therefore, we can suggest that fine-grained soil at Jezero crater contains some adsorbed water, which is consistent with the elevated H signature observed in LIBS data, and the fact that H is not correlated to any major elements.

Some mineralogical phases are particularly hygroscopic and can therefore adsorb some water, as measured at Gale crater with the SAM experiment (Leshin et al., 2013) and observed in LIBS data with ChemCam (Meslin et al., 2013; Cousin et al., 2017a). Laboratory experiments carried out under conditions similar to those in SAM showed that sulfates and perchlorates tend to adsorb water, as their temperature of water-release was relatively low (Bish et al., 1990). It has also been shown that small amounts of Fe sulfates (or even Ca chloride) can have a significant impact on water content due to their high adsorption capacity (Vakkada Ramachandran et al., 2021). Mg sulfates were detected in some bedrock from the crater floor (Meslin et al., 2022; Phua et al., 2023), even though they have not been detected in the fine-grained soil of Jezero by SuperCam (Figure S2 and Fig. 17). Nevertheless, a weak sulfate detection was made in SHERLOC data in the soil sample (Hausrath et al., 2023).

Anhydrous Na-perchlorates have been detected with SuperCam in some of the crater floor bedrock (Meslin et al., 2022; Wiens et al., 2022). Perchlorates have not been directly detected yet in SuperCam soil targets, but Cl is detected and correlated to the H signal. Hydrated perchlorates were detected in soil in previous in-situ missions, such as in the two Viking landing sites (Clark, 1993), in the arctic plains with Phoenix (Kounaves et al., 2014) and at Gale Crater (found in same proportions as at Phoenix soil Leshin et al., 2013). Even though such perchlorates have not yet been detected unambiguously in the soil at Jezero, modelling studies show that the stability of perchlorates at Jezero crater is longer than that of Gale crater (Li et al., 2022). Perchlorates are highly hygroscopic and can adsorb an important amount of water, playing an important role in the water content of soil (Hudson et al., 2009). In consequence, a small amount of sulfates and/or perchlorates (below our LOD) can be part of the fine-grained soil of Jezero crater.

In addition to the mineralogical phases that constitute the fine-grained soil, the Specific Surface Area (SSA) of the soil itself plays an important role in the soil's ability to retain exchangeable water. Indeed, it has been shown that the amount of H_2O adsorbed was relatively insensitive to the mineralogies (Meslin et al., 2013; Zent and Quinn, 1997). SSA of fine-grained soil targets at Gale crater has been estimated to less than 30–45 m^2g^{-1} (Meslin et al., 2013), using the results obtained between day/night experiments on the same soil target, as well as the water content measured by SAM and the relative humidity (RH) given by REMS. At Jezero, only one soil analysis was performed at night, with no significant change in the H signal in LIBS data. RH measured by MEDA is below 2% and therefore below the instrument sensitivity (Polkko et al., 2023). However, MEDA data acquired between 21:00 and 09:00 suggest that some changes in the soil hydration state could be possible (Hausrath et al., 2023; Polkko et al., 2023), as also observed with REMS at Gale (Savijärvi and Harri, 2021).

All these observations strongly suggest that the hydration of fine-grained soil at Jezero is mainly in the form of adsorbed water. Its content is driven by two factors: the presence of several hygroscopic phases, such as some sulfates and perchlorates, and also the SSA of the particles that constitute the soil.

4.4. Comparison to Gale crater

Fine-grained soil (<250 μm) contains the smallest particles that are transported by winds, which have been considered as representing a global component (Clark, 1993; Yen et al., 2005; Sullivan et al., 2010). This possibly global component is of particular interest to better constrain the different rock sources all over the planet, but also the different processes that have participated to the soil formation as we observe it today (i.e., alteration processes, atmosphere–surface exchanges, transport).

Therefore, our comparison between Jezero and Gale crater soil is based only on the fine-grained soil observed at both sites. The Curiosity rover has been exploring Gale crater for more than eleven years now, representing more than 3800 sols, with 125 targets (782 points) corresponding to fine-grained soil targets observed by the ChemCam instrument up to sol 3500. At Jezero, SuperCam has analysed 30 fine-grained soil targets up to sol 650, corresponding to 219 points. Fine-grained soil targets are compared between the two locations using their spectra directly, as one of the strengths of SuperCam and ChemCam is that they use the same analytical method (LIBS). In addition to direct spectral comparison, we use the ICA scores (see Section 2.3).

In order to make sure such a comparison was correct, we have acquired data from both instruments (ChemCam and SuperCam) in laboratory on the same targets. For this, we used the characterized SuperCam calibration targets (Manrique et al., 2020; Cousin et al., 2022c). ICA scores obtained from spectra acquired with ChemCam and SuperCam setups are shown in Fig. 19, where the red dashed line corresponds to the 1:1 comparison. ICA scores obtained from the ChemCam and SuperCam laboratory datasets are similar for several elements, such as for H and Ca in the UV range. For Mg, K, Si and Ca (UV and VNIR ranges), the ICA scores are in good agreement between the two datasets, but tend to be higher in SuperCam for the highest

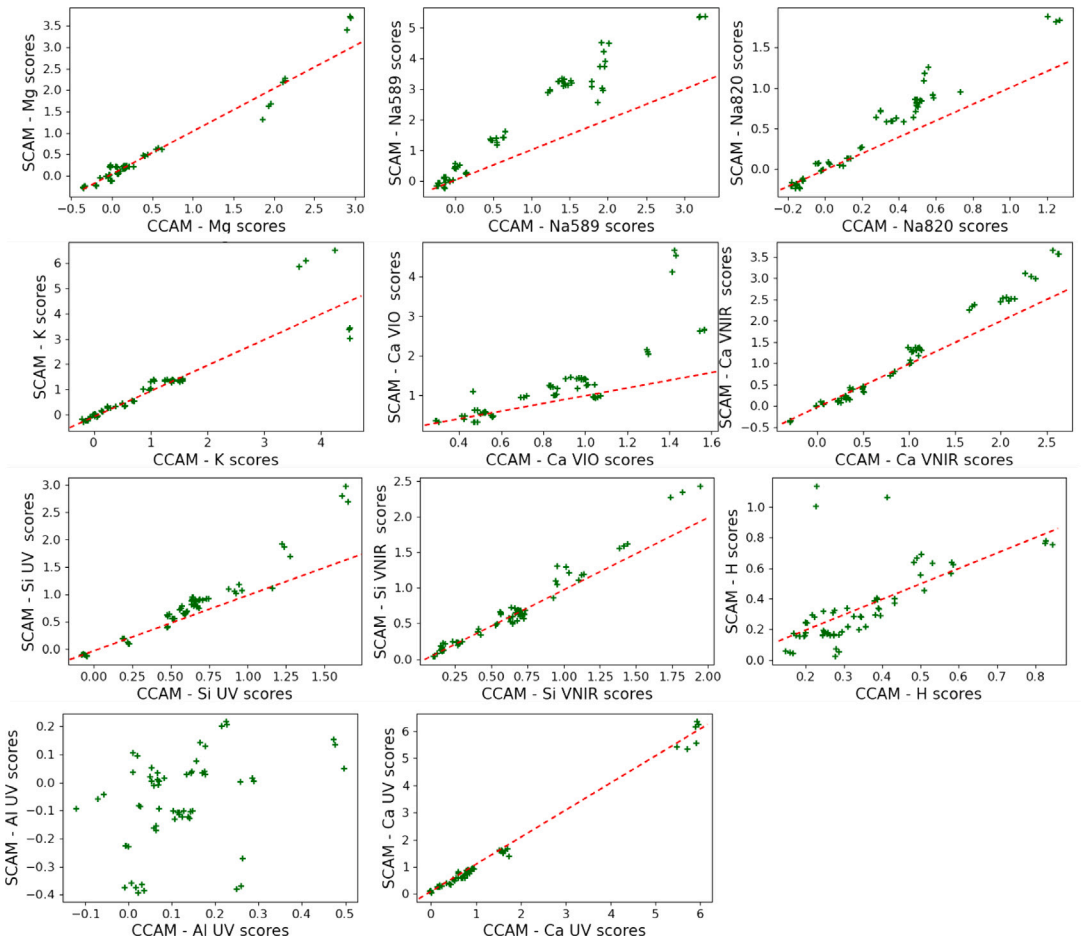

Fig. 19. ICA scores obtained from ChemCam (X axis) and SuperCam (Y axis) spectra on the SuperCam Calibration targets in laboratory. SuperCam calibration targets are used for several reasons: they have been acquired both with ChemCam and SuperCam setups, their composition is known as they are well characterized (Cousin et al., 2022c), and they have a wide range of content for each major elements. Red dashed line corresponds to the 1:1 comparison. These laboratory data as well as the ICA scores can be available via the Zenodo platform (see Data Availability Statement).

values. Moreover, there seems to be an instrumental bias for the Na scores from the Na line at 589 nm, which are systematically higher in the SuperCam dataset compared to the ChemCam one. Concerning the Na scores from the Na line at 820 nm, they are more consistent but higher in the SuperCam dataset for the higher ones. Therefore, only the scores obtained from Na at 820 nm will be used for the comparison between the two datasets, keeping in mind that for high values these could be overestimated for the SuperCam data. Finally, Al scores cannot be compared as there is no correlation obtained between the ChemCam and SuperCam laboratory data in Fig. 19.

The ICA scores from Mars data are presented in Fig. 20 for ChemCam (in green) and SuperCam (in orange) for all the major elements as well as for the H signal. First, it can be observed that the fine-grained soil from Gale crater shows more dispersion compared to that from Jezero. A few differences between the fine-grained soil from Gale and Jezero can be observed: 1/ data from Gale crater are more enriched in alkali (Na, K) compared to those observed at Jezero. The fact that the Na score tends to be overestimated in SuperCam data (see Fig. 19) suggests that the enrichment in Na in Gale data is even more important. 2/ Fine-grained soil from Jezero crater present in average more Mg compared to those from Gale, as well as slightly more H. Indeed, Mg vs H scores show two different distributions, suggesting that the soil at Jezero is more hydrated compared to those at Gale crater. In the SuperCam data, extreme high Mg scores do not have particularly high H scores, and could be undocumented buried pebbles. A few points are intermediate in both their Mg and H scores, and could correspond to some altered olivines as seen by PIXL (Hausrath et al., 2023). A few shots of the data acquired at Gale crater show some Ca enrichment, probably related to some Ca sulfate veins that are ubiquitous at Gale (Nachon et al., 2017).

Volatile elements such as Cl and S are difficult to compare using the ICA technique, as these elements present very small emission lines and therefore do not represent an important covariance between the spectra. Moreover, these elements are not routinely quantified yet, even though some quantitative models are being developed for S for the ChemCam data (Clegg et al., 2017; Rapin et al., 2019). Here we therefore compare directly the spectra obtained for each landing site. To do so, we calculated the average spectrum for the fine-grained soil from Jezero, the average spectrum from the fine-grained soil from Gale crater, along with the standard-deviation spectrum from each landing site. Also, we focused on the relevant spectral range where the Cl and S lines are observed (540–620 nm for the S lines, and 711–851 nm for Cl lines), and this spectral range is normalized to its total intensity to correct for the different intensities due to the different setups and possibly different distances. Fig. 21 is a close-up of these two elements' main emission lines. S lines are challenging because of their interferences with Fe lines, and therefore are expressed by a shallower dip between the Fe lines. It can be observed that the average spectrum from ChemCam data (in green) presents a shallower dip between the Fe lines compared to the average spectrum obtained at Jezero, even with a larger dispersion in the ChemCam data. This means that overall the S signal is higher in the ChemCam data. This can be observed mainly with the S lines at 543 nm and 545.4 nm, located on the shoulder of Fe lines. Concerning the Cl line, it is slightly higher in the SuperCam

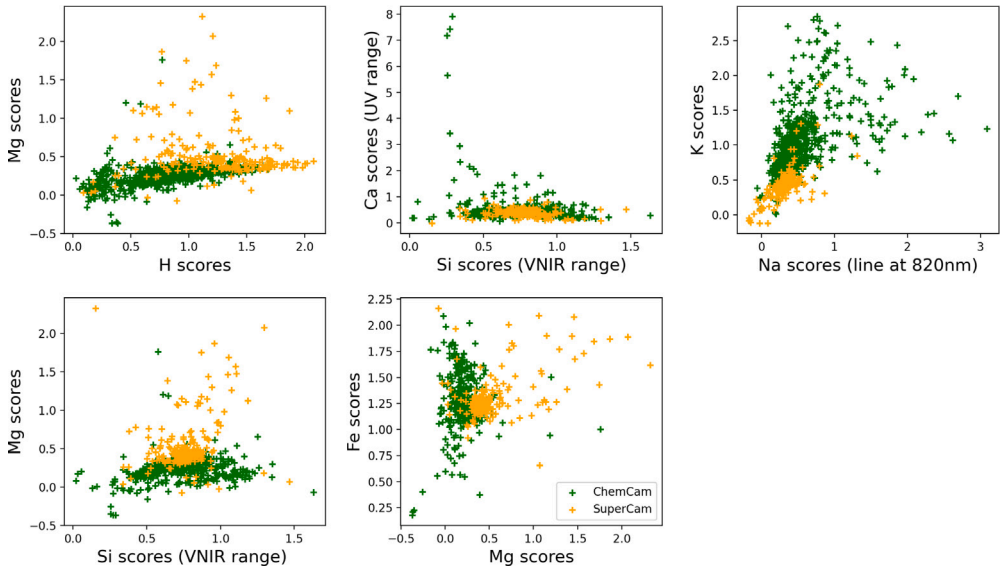

Fig. 20. ICA scores for each major element and H signal for both ChemCam (in green) and SuperCam (in orange) point-to-point fine-grained soil. The ICA scores obtained from both Mars dataset can be available via the Zenodo platform (see Data Availability Statement). (For interpretation of the references to colour in this figure legend, the reader is referred to the web version of this article.)

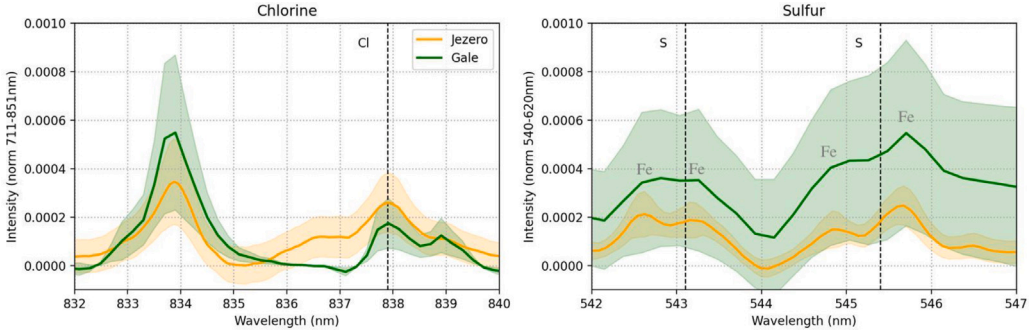

Fig. 21. Close-up of the LIBS spectral regions for the Cl line at 837.8 nm (left) and for some of the S lines (right). The green spectrum corresponds to the average spectrum of all the fine-grained soil analysed at Gale crater with ChemCam, whereas the orange one corresponds to the average spectrum of the fine-grained soil analysed by SuperCam at Jezero crater. The green and orange shadows correspond to the dispersion found in fine-grained soil at Gale and Jezero craters, respectively. Data have been normalized to the total intensity of the range. (For interpretation of the references to colour in this figure legend, the reader is referred to the web version of this article.)

average spectrum (orange), higher than the highest observation from Gale.

David et al. (2022) have shown that the amorphous component in the soil at Gale crater contains some hydrated Mg sulfates (and to a lesser extent, probably some Fe-sulfates too), which are probably the main carrier of the hydration of the soil at Gale crater. However, the fine-grained soil observed at Jezero do not seem to be enriched in Mg sulfates from Fig. 17, and the VISIR data do not show any presence of sulfates in the fine-grained soil either (Fig. 14). This could imply different weathering conditions at Jezero compared to Gale, where the Mg-sulfates are thought to come from the weathering of olivine in water-limited acidic conditions (David et al., 2022).

This comparison to Gale crater fine-grained soil targets shows that local contaminations are not only observed in the coarsest particles of the soil, but also in the fine-grained ones. Indeed, the average higher ICA scores for Mg in the fine-grained soil at Jezero compared to Gale (Fig. 20) can be explained by some local inputs from the erosion of the ubiquitous Mg-rich olivines (as well as of the pyroxenes) observed in bedrock of the crater floor and in the delta. The local influence can also be observed in the fine-grained soil from Gale crater, which shows higher ICA scores for Na, K, Al and Ca compared to fine-grained soil analysed at Jezero (Fig. 20). The enrichment in those elements comes from the erosion of the felsic float rocks or their pebbles. Moreover, Gale has been demonstrated to be particularly rich in Ca sulfate veins as these have been observed in most of the terrains traversed by the rover (Nachon et al., 2017). Therefore, the overall higher Ca ICA score observed in ChemCam fine-grained soil could also be related to the ubiquitous presence of Ca sulfate at Gale, which are not observed at Jezero. This would also be consistent with the fact that overall the fine-grained soil at Jezero contain less sulfur compared to those from Gale.

Finally, Jezero fine-grained soil targets seem to contain several components that contribute to this higher hydration compared to Gale. Amorphous material is hard to detect with Perseverance's payload. However, as discussed in 4.3, adsorbed water seems to play an important role concerning the water content in soil. Indeed, hygroscopic phases such as sulfates and perchlorates have been detected in the soil of Jezero (Hausrath et al., 2023), also in some bedrock targets (Phua et al., 2023; Meslin et al., 2022; Wiens et al., 2022). Their individual amount in the fine-grained soil might be too low though to be detected by the LIBS technique. The S signal is lower at Jezero, probably due to a lack of local inputs, as sulfate veins are scarce at this location. However, Cl signal is slightly more elevated at Jezero, in accordance to the presence of some perchlorates. This presence of salts is also

supported by the observation of some soil crust (Hausrath et al., 2023). Another factor that contributes to the high hydration of Jezero soil is the SSA of the grains. If we assume that the hydration of the Jezero fine-grained soil comes largely from adsorbed water, and that the RH during the day at Jezero is similar to that at Gale (around 0.1% Pommerol et al., 2009; Meslin et al., 2013), then we can deduce that the SSA of the grains that make up Jezero soil might be greater than at Gale. Fine-grained soil at Gale crater contains 1.5–3 wt% water (Leshin et al., 2013). Our observations suggest that 1.5–3 wt% is a lower limit for the Jezero fine-grained soil water content.

5. Conclusions

SuperCam has analysed a total of 343 LIBS points in soil targets up to sol 650 when the backup sample depot was created (Prepared by the MSR Campaign Science Group (MCSG)). Along the traverse, a majority of fine-grained (<250 μm) soil targets have been investigated (representing 59% of the points), with 29% of the dataset corresponding to gravels larger than 1 mm (very coarse sand grains, granules and larger gravels). These observations support the paucity of grains between 250 μm and 1 mm, related to the saltation effect that implies a greater grain attrition.

For the first time in-situ on Mars, soil targets have been analysed both with VISIR and LIBS techniques, with a very similar field of view (slightly larger for VISIR). The weak signature in VISIR data in fine-grained soil targets seem to be related to the grain size of these targets, as the LIBS data revealed a mixture of mainly primary phases, consistent with previous in-situ observations at Gale crater.

Contributions from erosion of local rocks are observed, both in the fine-grained and very coarse-grained (and larger) soil at Jezero. These very coarse grains and larger gravels (>1 mm) come mainly from local materials. Several coarse grains showed a clear signature of olivine similar to that of the crater floor bedrock. Several other very coarse grains from the delta front location showed instead a signature of Mg-rich phyllosilicates, as observed in the rocks of this location.

The fine-grained soil has a composition relatively close to that of the dust, with enrichment in mafic elements. Some very elevated Mg contents are observed in some shots, due to erosion of local rocks. On the other hand, Gale crater fine-grained soil is more enriched in Ca due to the ubiquitous presence of Ca sulfate veins at this location, which are very rare at Jezero up to sol 650.

Fine-grained soil targets, thought to represent a global component of Mars, seem to be composed mainly of a mixture of primary phases that depend on local bedrock. The global component therefore is related mainly to the finest particles, such as the dust.

Fine-grained soil targets are more hydrated at Jezero compared to Gale. This could be explained by several possible factors: 1. fine-grained soil is primarily made of a mixture of primary phases, but also contain some hygroscopic material such as some sulfates and perchlorates. They are below the SuperCam detection limits, but have been detected by SHERLOC; 2. the water is in the form of adsorbed water; 3. the specific surface area of the fine-grained material in soil at Jezero is higher than that of Gale crater. The water content in Jezero fine-grained soil has a lower limit at 1.5–3 wt %. Our measurements at Jezero and their comparison with results obtained at other landing sites (e.g. Gale crater) demonstrates that the carrier of hydration in the soil varies with the location. At Jezero crater the presence of X-ray amorphous material is hard to detect, but Mg sulfates are clearly less present (either amorphous or crystalline) in fine-grained soil compared to that at Gale crater.

CRediT authorship contribution statement

A. Cousin: Writing – review & editing, Writing – original draft, Methodology, Investigation, Formal analysis, Data curation, Conceptualization. **P.-Y. Meslin:** Writing – review & editing, Conceptualization. **O. Forni:** Writing – review & editing, Formal analysis. **O. Beyssac:** Writing – review & editing, Writing – original draft, Formal analysis. **E. Clavé:** Writing – review & editing, Formal analysis, Data curation. **E. Hausrath:** Conceptualization. **P. Beck:** Writing – review & editing. **E. Dehouck:** Writing – review & editing. **S. Schröder:** Writing – review & editing. **T. Fouchet:** Writing – review & editing. **C. Bedford:** Writing – review & editing. **J. Johnson:** Writing – review & editing. **P. Pilleri:** Visualization, Software, Formal analysis. **J. Lasue:** Writing – review & editing. **O. Gasnault:** Writing – review & editing. **N. Martin:** Formal analysis. **B. Chide:** Formal analysis. **A. Udry:** Writing – review & editing. **R. Sullivan:** Conceptualization. **A. Vaughan:** Conceptualization. **I. Poblacion:** Writing – review & editing. **G. Arana:** Writing – review & editing. **J.M. Madariaga:** Writing – review & editing. **S. Clegg:** Writing – review & editing. **S. Maurice:** Writing – review & editing, Validation. **R.C. Wiens:** Writing – review & editing, Validation.

Declaration of competing interest

The authors declare that they have no known competing financial interests or personal relationships that could have appeared to influence the work reported in this paper.

Data availability

All SuperCam and ChemCam data used in this study are publicly available on the Planetary Data System (http://pds-geosciences.wustl.edu/missions/msl/chemcam.htmand http://pds-geosciences.wustl.edu/missions/mars2020/supercam.htm). Laboratory data used for ICA validation, as well as the ICA scores retrieved from laboratory data, along with those from Mars data, can be found in the Zenodo open-source online repository (https://zenodo.org/records/13118478?preview=1&token=eyJhbGciOiJIUzUxMiJ9.eyJpZCI6IjIwYjNiMThkLTAzN2QtNDRkNi05M2E1LTlmNjhlZGIxNmVlNSIsImRhdGEiOnt9LCJyYW5kb20iOiI5MDc3ZTY3N2I1OWM1NDBmZGIyMjU0NjIyZTc1MTJmNSJ9.NFk2gCZ91D6s4Kcpto_2BESpXa1oV2nPVC64UUFy5Fo0TVoH4ScHU_bszyWhaS76NSnH4nA2mmTRxqTpUnYp9g).

Acknowledgements

NASA contract NNH13ZDA018O to LANL and Purdue. Many people helped with this project in addition to the co-authors, including hardware and operation teams, and we are most grateful for their support. This project is conducted in France under the authority of CNES. We would like to thank the two reviewers to have helped us improve our manuscript.

Appendix A. Supplementary data

Supplementary material related to this article can be found online at https://doi.org/10.1016/j.icarus.2024.116299.

References

Allwood, A.C., Wade, L.A., Foote, M.C., Elam, W.T., Hurowitz, J.A., Battel, S., Dawson, D.E., Denise, R.W., Ek, E.M., Gilbert, M.S., et al., 2020. PIXL: Planetary instrument for X-ray lithochemistry. Space Sci. Rev. 216, 1–132.

Anderson, R.B., Forni, O., Clegg, S.M., Cousin, A., Frydenvang, J., Pilleri, P., Legett, C., Wiens, R.C., Maurice, S., Arana, G., Beyssac, O., Bousquet, B., Chide, B., Clave, E., Delapp, D., Essunfeld, A., Fouchet, T., Garcia-Florentino, C., Gasnault, O., Gibbons, E., Laserna, J., Lasue, J., Manrique, J.A., Madariaga, J.M., Newell, R., Ollila, A., Sharma, S., Simon, J., Sobron, P., 2021. SuperCam Laser Induced Breakdown Spectroscopy (LIBS) data processing, calibration, and first results. In: Lunar and Planetary Science Conference. p. 1606.

Anderson, R.B., Forni, O., Cousin, A., Wiens, R.C., Clegg, S.M., Frydenvang, J., Gabriel, T.S., Ollila, A., Schröder, S., Beyssac, O., et al., 2022. Post-landing major element quantification using SuperCam laser induced breakdown spectroscopy. Spectrochim. Acta B: Atom. Spectrosc. 188, 106347.

Arvidson, R.E., Ashley, J.W., Bell III, J.F., Chojnacki, M., Cohen, J., Economou, T.E., Farrand, W.H., Fergason, R., Fleischer, I., Geissler, P., Gellert, R., Golombek, M.P., Grotzinger, J.P., Guinness, E.A., Haberle, R.M., Herkenhoff, K.E., Herman, J.A., Iagnemma, K.D., Jolliff, B.L., Johnson, J.R., Klingelhöfer, G., Knoll, A.H., Knudson, A.T., Li, R., McLennan, S.M., Mittlefehldt, D.W., Morris, R.V., Parker, T.J., Rice, M.S., Schröder, C., Soderblom, L.A., Squyres, S.W., Sullivan, R.J., Wolff, M.J., 2011. Opportunity Mars rover mission: Overview and selected results from Purgatory ripple to traverses to endeavour crater. J. Geophys. Res.: Planets 116 (E7), http://dx.doi.org/10.1029/2010JE003746.

Arvidson, R.E., Bell III, J.F., Bellutta, P., Cabrol, N.A., Catalano, J.G., Cohen, J., Crumpler, L.S., Des Marais, D.J., Estlin, T.A., Farrand, W.H., Gellert, R., Grant, J.A., Greenberger, R.N., Guinness, E.A., Herkenhoff, K.E., Herman, J.A., Iagnemma, K.D., Johnson, J.R., Klingelhöfer, G., Li, R., Lichtenberg, K.A., Maxwell, S.A., Ming, D.W., Morris, R.V., Rice, M.S., Ruff, S.W., Shaw, A., Siebach, K.L., de Souza, P.A., Stroupe, A.W., Squyres, S.W., Sullivan, R.J., Talley, K.P., Townsend, J.A., Wang, A., Wright, J.R., Yen, A.S., 2010. Spirit Mars rover mission: Overview and selected results from the northern home plate winter haven to the side of Scamander crater. J. Geophys. Res.: Planets 115 (E7), http://dx.doi.org/10.1029/2010JE003633.

Bell, J., Maki, J., Mehall, G., Ravine, M., Caplinger, M., Bailey, Z., Brylow, S., Schaffner, J., Kinch, K., Madsen, M., et al., 2021. The Mars 2020 perseverance rover mast camera zoom (Mastcam-Z) multispectral, stereoscopic imaging investigation. Space Sci. Rev. 217, 1–40.

Beyssac, O., Forni, O., Cousin, A., Udry, A., Kah, L.C., Mandon, L., Clavé, O.E., Liu, Y., Poulet, F., Quantin Nataf, C., Gasnault, O., Johnson, J.R., Benzerara, K., Beck, P., Dehouck, E., Mangold, N., Alvarez Llamas, C., Anderson, R.B., Arana, G., Barnes, R., Bernard, S., Bosak, T., Brown, A.J., Castro, K., Chide, B., Clegg, S.M., Cloutis, E., Fouchet, T., Gabriel, T., Gupta, S., Lacombe, G., Lasue, J., Le Mouelic, S., Lopez-Reyes, G., Madariaga, J.M., McCubbin, F.M., McLennan, S.M., Manrique, J.A., Meslin, P.Y., Montmessin, F., Núñez, J., Ollila, A.M., Ostwald, A., Pilleri, P., Pinet, P., Royer, C., Sharma, S.K., Schröder, S., Simon, J.I., Toplis, M.J., Veneranda, M., Willis, P.A., Maurice, S., Wiens, R.C., The SuperCam Team, 2023a. Petrological traverse of the Olivine Cumulate Séítah Formation at Jezero Crater, Mars: A perspective from SuperCam onboard perseverance. J. Geophys. Res.: Planets 128 (7), http://dx.doi.org/10.1029/2022JE007638, e2022JE007638 2022JE007638.

Beyssac, O., Forni, O., Cousin, A., Udry, A., Kah, L., Mandon, L., Clavé, E., Liu, Y., Poulet, F., Quantin Nataf, C., et al., 2023b. Petrological traverse of the olivine cumulate Séítah formation at Jezero crater, Mars: A perspective from SuperCam onboard perseverance. J. Geophys. Res.: Planets e2022JE007638.

Bhartia, R., Beegle, L.W., DeFlores, L., Abbey, W., Razzell Hollis, J., Uckert, K., Monacelli, B., Edgett, K.S., Kennedy, M.R., Sylvia, M., et al., 2021. Perseverance's scanning habitable environments with Raman and luminescence for organics and chemicals (SHERLOC) investigation. Space Sci. Rev. 217 (4), 58.

Bish, D.L., Stucki, J., Mumpto, F., 1990. Thermal Analysis in Clay Science, vol. 3, Clay Minerals Society Boulder.

Blake, D.F., Morris, R.V., Kocurek, G., Morrison, S., Downs, R.T., Bish, D., Ming, D., Edgett, K., Rubin, D., Goetz, W., et al., 2013. Curiosity at Gale crater, Mars: Characterization and analysis of the rocknest sand shadow. Science 341 (6153), 1239505.

Blake, D., Vaniman, D., Achilles, C., Anderson, R., Bish, D., Bristow, T., Chen, C., Chipera, S., Crisp, J., Des Marais, D., et al., 2012. Characterization and calibration of the CheMin mineralogical instrument on Mars science laboratory. Space Sci. Rev. 170, 341–399.

Cardoso, J.-F., Souloumiac, A., 1993. Blind beamforming for non-Gaussian signals. In: IEE Proceedings F (Radar and Signal Processing), vol. 140, (no. 6), IET, pp. 362–370.

Certini, G., Karunatillake, S., Zhao, Y.-Y.S., Meslin, P.-Y., Cousin, A., Hood, D.R., Scalenghe, R., 2020. Disambiguating the soils of Mars. Planet. Space Sci. (ISSN: 0032-0633) 186, 104922. http://dx.doi.org/10.1016/j.pss.2020.104922.

Chide, B., Murdoch, N., Bury, Y., Maurice, S., Jacob, X., Merrison, J.P., Iversen, J.J., Meslin, P.-Y., Bassas-PortÃs, M., Cadu, A., Sournac, A., Dubois, B., Lorenz, R.D., Mimoun, D., Wiens, R.C., 2020. Experimental wind characterization with the SuperCam microphone under a simulated Martian atmosphere. Icarus (ISSN: 0019-1035) 114060. http://dx.doi.org/10.1016/j.icarus.2020.114060.

Clark, B.C., 1993. Geochemical components in Martian soil. Geochim. Cosmochim. Acta (ISSN: 0016-7037) 57 (19), 4575–4581. http://dx.doi.org/10.1016/0016-7037(93)90183-W.

Clavé, E., Benzerara, K., Beck, P., Meslin, P.-Y., Beyssac, O., Forni, O., Cousin, A., Bosak, T., Bousquet, B., Castro, K., et al., 2022. Carbonate detection with supercam in the Jezero crater, Mars. In: 53rd Lunar and Planetary Science Conference, (no. 2678), p. 2001.

Clegg, S.M., Anderson, R.B., Frydenvang, J., Forni, O., Newsom, H.E., Blaney, D.L., Maurice, S., Wiens, R.C., 2017. Sulfur geochemical analysis and interpretation with ChemCam on the curiosity rover. In: AGU Fall Meeting Abstracts, vol. 2017, pp. P31A–2796.

Clegg, S.M., Wiens, R.C., Anderson, R., Forni, O., Frydenvang, J., Lasue, J., Cousin, A., Payre, V., Boucher, T., Dyar, M.D., et al., 2017. Recalibration of the Mars science laboratory ChemCam instrument with an expanded geochemical database. Spectrochim. Acta B: Atom. Spectrosc. 129, 64–85.

Comon, P., 1994. Independent component analysis, A new concept? Signal Process. (ISSN: 0165-1684) 36 (3), 287–314, Higher Order Statistics.

Cousin, A., Dehouck, E., Meslin, P.-Y., Forni, O., Williams, A.J., Stein, N., Gasnault, O., Bridges, N., Ehlmann, B., Schröder, S., Payré, V., Rapin, W., Pinet, P., Sautter, V., Lanza, N., Lasue, J., Maurice, S., Wiens, R.C., 2017a. Geochemistry of the Bagnold dune field as observed by ChemCam and comparison with other aeolian deposits at Gale Crater. J. Geophys. Res.: Planets 122 (10), 2144–2162. http://dx.doi.org/10.1002/2017JE005261.

Cousin, A., Dehouck, E., Meslin, P.-Y., Forni, O., Williams, A.J., Stein, N., Gasnault, O., Bridges, N., Ehlmann, B., Schröder, S., et al., 2017b. Geochemistry of the Bagnold dune field as observed by ChemCam and comparison with other aeolian deposits at Gale Crater. J. Geophys. Res.: Planets 122 (10), 2144–2162.

Cousin, A., Meslin, P.Y., Dehouck, E., David, G., Lasue, J., Forni, O., Schröder, S., Wiens, R., Maurice, S., Gasnault, O., Lanza, N., 2022a. Classification of soils at Gale along the traverse: A ChemCam perspective. In: Lunar and Planetary Science Conference. vol. 53, Lunar and Planetary Institute, The Woodlands, TX, United States, p. 1258, URL https://hal.archives-ouvertes.fr/hal-03847339.

Cousin, A., Meslin, P., Dehouck, E., David, G., Lasue, J., Forni, O., Schröder, S., Wiens, R., Maurice, S., Gasnault, O., et al., 2022b. Classification of soils at Gale along the traverse. In: Lunar and Planetary Science Conference, vol. 53, p. 1258.

Cousin, A., Meslin, P., Wiens, R., Rapin, W., Mangold, N., Fabre, C., Gasnault, O., Forni, O., Tokar, R., Ollila, A., et al., 2015. Compositions of coarse and fine particles in Martian soils at Gale: A window into the production of soils. Icarus 249, 22–42.

Cousin, A., Sautter, V., Fabre, C., Dromart, G., Montagnac, G., Drouet, C., Meslin, P., Gasnault, O., Beyssac, O., Bernard, S., et al., 2022c. SuperCam calibration targets on board the perseverance rover: Fabrication and quantitative characterization. Spectrochim. Acta B: Atom. Spectrosc. 188, 106341.

David, G., Dehouck, E., Meslin, P.-Y., Rapin, W., Cousin, A., Forni, O., Gasnault, O., Lasue, J., Mangold, N., Beck, P., et al., 2022. Evidence for amorphous sulfates as the main carrier of soil hydration in Gale crater, Mars. Geophys. Res. Lett. 49 (21), e2022GL098755.

David, G., Meslin, P.-Y., Dehouck, E., Gasnault, O., Cousin, A., Forni, O., Berger, G., Lasue, J., Pinet, P., Wiens, R., et al., 2021. Laser-Induced Breakdown Spectroscopy (LIBS) characterization of granular soils: Implications for ChemCam analyses at Gale crater, Mars. Icarus 365, 114481.

Dehouck, E., Forni, O., Quantin-Nataf, C., Beck, P., Mangold, N., Royer, C., Clavé, E., Beyssac, O., Johnson, J.R., Mandon, L., et al., 2023. Overview of the bedrock geochemistry and mineralogy observed by supercam during perseverance's delta front campaign. In: 54th Lunar and Planetary Science Conference, vol. 54, p. 2862.

Ehlmann, B., Edgett, K., Sutter, B., Achilles, C., Litvak, M., Lapotre, M., Sullivan, R., Fraeman, A., Arvidson, R., Blake, D., et al., 2017. Chemistry, mineralogy, and grain properties at Namib and High dunes, Bagnold dune field, Gale crater, Mars: A synthesis of curiosity rover observations. J. Geophys. Res.: Planets 122 (12), 2510–2543.

Farley, K., Stack, K., Shuster, D., Horgan, B., Hurowitz, J., Tarnas, J., Simon, J., Sun, V., Scheller, E., Moore, K., et al., 2022. Aqueously altered igneous rocks sampled on the floor of Jezero crater, Mars. Science 377 (6614), eabo2196.

Farley, K., Williford, K., Stack, K., Bhartia, R., Chen, A., de la Torre, M., Hand, K., Goreva, Y., Herd, C., Hueso, R., Liu, Y., Maki, J., Martinez, G., Moeller, R., Nelessen, A., Newman, C., Nunes, D., Ponce, A., Spanovich, N., Willis, P., Beegle, L., Bell, J., Brown, A., Hamran, S., Hurowitz, J., Maurice, S., Paige, D., Rodriguez-Manfredi, J., Schulte, M., Wiens, R., 2020. Mars 2020 mission overview. Space Sci. Rev. (ISSN: 0038-6308) 216 (8), http://dx.doi.org/10.1007/s11214-020-00762-y, Publisher Copyright: © 2020, Springer Nature B.V.

Forni, O., Bedford, C., Royer, C., Liu, Y., Wiens, R.C., Dehouck, E., Meslin, P.-Y., Udry, A., Beyssac, O., Gabriel, T.S., Beck, P., Gasnault, O., Quantin-Nataf, C., Johnson, J.R., Schröder, S., Pilleri, P., Debaille, V., Manelsy, H.T., Clark, B.C., Cousin, A., Maurice, S., Clegg, S.M., 2024. Nickel-copper deposits on Mars? Discovery of ore-grade abundances, and implications on formation and alteration. In: Lunar and Planetary Science Conference. p. 1236.

Forni, O., Bedford, C.C., Royer, C., Liu, Y., Wiens, R.C., Dehouck, E., Meslin, P.-Y., Udry, A., Beyssac, O., Gabriel, T.S., Beck, P., Gasnault, O., Quantin-Nataf, C., Johnson, J.R., Schröder, S., Pilleri, P., Debaille, V., Manelsy, H.T., Clark, B.C., Cousin, A., Maurice, S., Clegg, S.M., 2024. Nickel-copper deposits on mars? discovery of ore-grade abundances, and implications on formation and alteration. In: LPI Contributions. vol. 3040, p. 1236.

Forni, O., Maurice, S., Gasnault, O., Wiens, R.C., Cousin, A., Clegg, S.M., Sirven, J.-B., Lasue, J., 2013. Independent component analysis classification of laser induced breakdown spectroscopy spectra. Spectrochim. Acta B: Atom. Spectrosc. (ISSN: 0584-8547) 86, 31–41. http://dx.doi.org/10.1016/j.sab.2013.05.003.

Fouchet, T., Reess, J.-M., Montmessin, F., Hassen-Khodja, R., Nguyen-Tuong, N., Humeau, O., Jacquinod, S., Lapauw, L., Parisot, J., Bonafous, M., et al., 2022. The SuperCam infrared spectrometer for the perseverance rover of the Mars2020 mission. Icarus 373, 114773.

Fraeman, A., Ehlmann, B., Arvidson, R., Edwards, C., Grotzinger, J., Milliken, R., Quinn, D., Rice, M., 2016. The stratigraphy and evolution of lower mount sharp from spectral, morphological, and thermophysical orbital data sets. J. Geophys. Res.: Planets 121 (9), 1713–1736.

Gabriel, T.S.J., Anderson, R.B., Wiens, R., 2023. Dynamic uncertainty estimation of LIBS chemistry on Mars with Gaussian process regression. In: LPI Contributions, vol. 2806, p. 2189.

Gasnault, O., Virmontois, C., Maurice, S., Wiens, R.C., Le Mouelic, S., Bernardi, P., Forni, O., Pilleri, P., Daydou, Y., Rapin, W., Cais, P., 2021. A first look at the SuperCam RMI images aboard Perseverance. In: EGU General Assembly Conference Abstracts. pp. EGU21–16461. http://dx.doi.org/10.5194/egusphere-egu21-16461.

Hausrath, E., Adcock, C., Bechtold, A., Beck, P., Benison, K., Brown, A., Cardarelli, E., Carman, N.A., Chide, B., Christian, J., et al., 2023. An examination of soil crusts on the floor of Jezero crater, Mars. J. Geophys. Res.: Planets e2022JE007433.

Hausrath, E.M., Sullivan, R., Goreva, Y., Zorzano, M.P., Cardarelli, E., Vaughan, A., Cousin, A., Siljestrom, S., Shumway, A., VanBommel, S., Martinez, G., Johnson, J., Bechtold, A., Paar, G., Poulet, F., Herd, C.D.K., Benison, K., Sephton, M., Madariaga, J.M., Lasue, J., Wiens, R.C., Martinez-Frias, J., Bell, J.F., Czaja, A.D., Adcock, C.T., Randazzo, N., 2023. The first regolith samples from Mars. In: LPI Contributions, vol. 2806, p. 2379.

Hudson, T.L., Aharonson, O., Schorghofer, N., 2009. Laboratory experiments and models of diffusive emplacement of ground ice on Mars. J. Geophys. Res.: Planets 114 (E1), http://dx.doi.org/10.1029/2008JE003149.

King, T.V., Ridley, W.I., 1987. Relation of the spectroscopic reflectance of olivine to mineral chemistry and some remote sensing implications. J. Geophys. Res.: Solid Earth 92 (B11), 11457–11469.

Kounaves, S.P., Chaniotakis, N.A., Chevrier, V.F., Carrier, B.L., Folds, K.E., Hansen, V.M., McElhoney, K.M., O'Neil, G.D., Weber, A.W., 2014. Identification of the perchlorate parent salts at the Phoenix Mars landing site and possible implications. Icarus 232, 226–231.

Lasue, J., Meslin, P., Cousin, A., Forni, O., Anderson, R., Beck, P., Beyssac, O., Brown, A., Clegg, S., Dehouck, E., et al., 2023. Supercam first shots: dust composition and variability. In: 54th Lunar and Planetary Science Conference 2023, vol. 54, p. 2244.

Lasue, J., Wiens, R., Stepinski, T., Forni, O., Clegg, S., Maurice, S., Team, C., 2011. Nonlinear mapping technique for data visualization and clustering assessment of LIBS data: Application to ChemCam data. Anal. Bioanal. Chem. 400, 3247–3260.

Leshin, L.A., Mahaffy, P.R., Webster, C.R., Cabane, M., Coll, P., Conrad, P.G., Archer, P.D., Atreya, S.K., Brunner, A.E., Buch, A., Eigenbrode, J.L., Flesch, G.J., Franz, H.B., Freissinet, C., Glavin, D.P., McAdam, A.C., Miller, K.E., Ming, D.W., Morris, R.V., Navarro-González, R., Niles, P.B., Owen, T., Pepin, R.O., Squyres, S., Steele, A., Stern, J.C., Summons, R.E., Sumner, D.Y., Sutter, B., Szopa, C., Teinturier, S., Trainer, M.G., Wray, J.J., Grotzinger, J.P., Team, M.S., Kemppinen, O., Bridges, N., Johnson, J.R., Minitti, M., Cremers, D., Bell, J.F., Edgar, L., Farmer, J., Godber, A., Wadhwa, M., Wellington, D., McEwan, I., Newman, C., Richardson, M., Charpentier, A., Peret, L., King, P., Blank, J., Weigle, G., Schmidt, M., Li, S., Milliken, R., Robertson, K., Sun, V., Baker, M., Edwards, C., Ehlmann, B., Farley, K., Griffes, J., Miller, H., Newcombe, M., Pilorget, C., Rice, M., Siebach, K., Stack, K., Stolper, E., Brunet, C., Hipkin, V., Léveillé, R., Marchand, G., Sánchez, P.S., Favot, L., Cody, G., Flückiger, L., Lees, D., Nefian, A., Martin, M., Gailhanou, M., Westall, F., Israël, G., Agard, C., Baroukh, J., Donny, C., Gaboriaud, A., Guillemot, P., Lafaille, V., Lorigny, E., Paillet, A., Pérez, R., Saccoccio, M., Yana, C., Armiens-Aparicio, C., Rodríguez, J.C., Blázquez, I.C., Gómez, F.G., Gómez-Elvira, J., Hettrich, S., Malvitte, A.L., Jiménez, M.M., Martínez-Frías, J., Martín-Soler, J., Martín-Torres, F.J., Jurado, A.M., Mora-Sotomayor, L., Caro, G.M., López, S.N., Peinado-González, V., Pla-García, J., Manfredi, J.A.R., Romeral-Planelló, J.J., Fuentes, S.A.S., Martinez, E.S., Redondo, J.T., Urqui-O'Callaghan, R., Mier, M.-P.Z., Chipera, S., Lacour, J.-L., Mauchien, P., Sirven, J.-B., Manning, H., Fairén, A., Hayes, A., Joseph, J., Sullivan, R., Thomas, P., Dupont, A., Lundberg, A., Melikechi, N., Mezzacappa, A., DeMarines, J., Grinspoon, D., Reitz, G., Prats, B., Atlaskin, E., Genzer, M., Harri, A.-M., Haukka, H., Kahanpää, H., Kauhanen, J., Kemppinen, O., Paton, M., Polkko, J., Schmidt, W., Siili, T., Fabre, C., Wilhelm, M.B., Poitrasson, F., Patel, K., Gorevan, S., Indyk, S., Paulsen, G., Gupta, S., Bish, D., Schieber, J., Gondet, B., Langevin, Y., Geffroy, C., Baratoux, D., Berger, G., Cros, A., d'Uston, C., Forni, O., Gasnault, O., Lasue, J., Lee, Q.-M., Maurice, S., Meslin, P.-Y., Pallier, E., Parot, Y., Pinet, P., Schröder, S., Toplis, M., Lewin, É., Brunner, W., Heydari, E., Achilles, C., Oehler, D., Coscia, D., Israël, G., Dromart, G., Robert, F., Sautter, V., Mouélic, S.L., Mangold, N., Nachon, M., Stalport, F., François, P., Raulin, F., Cameron, J., Clegg, S., Cousin, A., DeLapp, D., Dingler, R., Jackson, R.S., Johnstone, S., Lanza, N., Little, C., Nelson, T., Wiens, R.C., Williams, R.B., Jones, A., Kirkland, L., Treiman, A., Baker, B., Cantor, B., Caplinger, M., Davis, S., Duston, B., Edgett, K., Fay, D., Hardgrove, C., Harker, D., Herrera, P., Jensen, E., Kennedy, M.R., Krezoski, G., Krysak, D., Lipkaman, L., Malin, M., McCartney, E., McNair, S., Nixon, B., Posiolova, L., Ravine, M., Salamon, A., Saper, L., Stoiber, K., Supulver, K., Beek, J.V., Beek, T.V., Zimdar, R., French, K.L., Iagnemma, K., Goesmann, F., Goetz, W., Hviid, S., Johnson, M., Lefavor, M., Lyness, E., Breves, E., Dyar, M.D., Fassett, C., Blake, D.F., Bristow, T., DesMarais, D., Edwards, L., Haberle, R., Hoehler, T., Hollingsworth, J., Kahre, M., Keely, L., McKay, C., Wilhelm, M.B., Bleacher, L., Brinckerhoff, W., Choi, D., Dworkin, J.P., Floyd, M., Garvin, J., Harpold, D., Jones, A., Martin, D.K., Pavlov, A., Raaen, E., Smith, M.D., Tan, F., Meyer, M., Posner, A., Voytek, M., Anderson, R.C., Aubrey, A., Beegle, L.W., Behar, A., Blaney, D., Brinza, D., Calef, F., Christensen, L., Crisp, J.A., DeFlores, L., Ehlmann, B., Feldman, J., Feldman, S., Hurowitz, J., Jun, I., Keymeulen, D., Maki, J., Mischna, M., Morookian, J.M., Parker, T., Pavri, B., Schoppers, M., Sengstacken, A., Simmonds, J.J., Spanovich, N., de la Torre Juarez, M., Vasavada, A.R., Yen, A., Cucinotta, F., Jones, J.H., Rampe, E., Nolan, T., Fisk, M., Radziemski, L., Barraclough, B., Bender, S., Berman, D., Dobrea, E.N., Tokar, R., Vaniman, D., Williams, R.M.E., Yingst, A., Lewis, K., Cleghorn, T., Huntress, W., Manhès, G., Hudgins, J., Olson, T., Stewart, N., Sarrazin, P., Grant, J., Vicenzi, E., Wilson, S.A., Bullock, M., Ehresmann, B., Hamilton, V., Hassler, D., Peterson, J., Rafkin, S., Zeitlin, C., Fedosov, F., Golovin, D., Karpushkina, N., Kozyrev, A., Litvak, M., Malakhov, A., Mitrofanov, I., Mokrousov, M., Nikiforov, S., Prokhorov, V., Sanin, A., Tretyakov, V., Varenikov, A., Vostrukhin, A., Kuzmin, R., Clark, B., Wolff, M., McLennan, S., Botta, O., Drake, D., Bean, K., Lemmon, M., Schwenzer, S.P., Anderson, R.B., Herkenhoff, K., Lee, E.M., Sucharski, R., Hernández, M.Á.d., Ávalos, J.J.B., Ramos, M., Kim, M.-H., Malespin, C., Plante, I., Muller, J.-P., Ewing, R., Boynton, W., Downs, R., Fitzgibbon, M., Harshman, K., Morrison, S., Dietrich, W., Kortmann, O., Palucis, M., Williams, A., Lugmair, G., Wilson, M.A., Rubin, D., Jakosky, B., Balic-Zunic, T., Frydenvang, J., vgaard Jensen, J.K., Kinch, K., Koefoed, A., Madsen, M.B., Stipp, S.L.S., Boyd, N., Campbell, J.L., Gellert, R., Perrett, G., Pradler, I., VanBommel, S., Jacob, S., Rowland, S., Atlaskin, E., Savijärvi, H., Boehm, E., Böttcher, S., Burmeister, S., Guo, J., Köhler, J., García, C.M., Mueller-Mellin, R., Wimmer-Schweingruber, R., Bridges, J.C., McConnochie, T., Benna, M., Bower, H., Blau, H., Boucher, T., Carmosino, M., Elliott, H., Halleaux, D., Rennó, N., Wong, M., Elliott, B., Spray, J., Thompson, L., Gordon, S., Newsom, H., Ollila, A., Williams, J., Vasconcelos, P., Bentz, J., Nealson, K., Popa, R., Kah, L.C., Moersch, J., Tate, C., Day, M., Kocurek, G., Hallet, B., Sletten, R., Francis, R., McCullough, E., Cloutis, E., ten Kate, I.L., Kuzmin, R., Arvidson, R., Fraeman, A., Scholes, D., Slavney, S., Stein, T., Ward, J., Berger, J., Moores, J.E., 2013. Volatile, isotope, and organic analysis of Martian fines with the Mars curiosity rover. Science 341 (6153), 1238937. http://dx.doi.org/10.1126/science.1238937.

Li, D., Zhao, Y.-Y.S., Meslin, P.-Y., Vals, M., Forget, F., Wu, Z., 2022. Cryogenic origin of fractionation between perchlorate and chloride under modern Martian climate. Commun. Earth Environ. 3 (1), 15.

Liu, Y., Tice, M., Schmidt, M., Treiman, A., Kizovski, T., Hurowitz, J., Allwood, A., Henneke, J., Pedersen, D., VanBommel, S., et al., 2022. An olivine cumulate outcrop on the floor of Jezero crater, Mars. Science 377 (6614), 1513–1519.

Mahaffy, P.R., Webster, C.R., Cabane, M., Conrad, P.G., Coll, P., Atreya, S.K., Arvey, R., Barciniak, M., Benna, M., Bleacher, L., et al., 2012. The sample analysis at Mars investigation and instrument suite. Space Sci. Rev. 170, 401–478.

Mandon, L., Quantin-Nataf, C., Royer, C., Beck, P., Fouchet, T., Johnson, J.R., Dehouck, E., Le Mouélic, S., Poulet, F., Montmessin, F., Pilorget, C., Gasnault, O., Forni, O., Mayhew, L.E., Beyssac, O., Bertrand, T., Clavé, E., Pinet, P., Brown, A.J., Legett, C., Tarnas, J., Cloutis, E.A., Poggiali, G., Fornaro, T., Maurice, S., Wiens, R.C., 2023. Reflectance of Jezero crater floor: 2. Mineralogical interpretation. J. Geophys. Res. (Planets) 128 (7), http://dx.doi.org/10.1029/2022JE007450, e2022JE007450.

Mandon, L., Quantin-Nataf, C., Thollot, P., Mangold, N., Lozac'h, L., Dromart, G., Beck, P., Dehouck, E., Breton, S., Millot, C., Volat, M., 2020. Refining the age, emplacement and alteration scenarios of the olivine-rich unit in the Nili Fossae region, Mars. Icarus (ISSN: 0019-1035) 336, 113436. http://dx.doi.org/10.1016/j.icarus.2019.113436.

Mangold, N., Gupta, S., Gasnault, O., Dromart, G., Tarnas, J., Sholes, S., Horgan, B., Quantin-Nataf, C., Brown, A., Le Mouélic, S., et al., 2021. Perseverance rover reveals an ancient delta-lake system and flood deposits at Jezero crater, Mars. Science 374 (6568), 711–717.

Manrique, J.A., Lopez-Reyes, G., Cousin, A., Rull, F., Maurice, S., Wiens, R.C., Madsen, M.B., Madariaga, J.M., Gasnault, O., Aramendia, J., Arana, G., Beck, P., Bernard, S., Bernardi, P., Bernt, M.H., Berrocal, A., Beyssac, O., Caïs, P., Castro, C., Castro, K., Clegg, S.M., Cloutis, E., Dromart, G., Drouet, C., Dubois, B., Escribano, D., Fabre, C., Fernandez, A., Forni, O., Garcia-Baonza, V., Gontijo, I., Johnson, J., Laserna, J., Lasue, J., Madsen, S., Mateo-Marti, E., Medina, J., Meslin, P.Y., Montagnac, G., Moral, A., Moros, J., Ollila, A.M., Ortega, C., Prieto-Ballesteros, O., Reess, J.M., Robinson, S., Rodriguez, J., Saiz, J., Sanz-Arranz, J.A., Sard, I., Sautter, V., Sobron, P., Toplis, M., Veneranda, M., 2020. SuperCam calibration targets: Design and development. Space Sci. Rev. 216 (8), 138. http://dx.doi.org/10.1007/s11214-020-00764-w.

Manrique, J.A., Lopez-Reyes, G., Cousin, A., Rull, F., Maurice, S., Wiens, R.C., Madsen, M., Madariaga, J.M., Gasnault, O., Aramendia, J., et al., 2020. SuperCam calibration targets: Design and development. Space Sci. Rev. 216, 1–27.

Martin, N.D., Chide, B., Sheridan, A., Cousin, A., Hausrath, E., Beyssac, O., Wiens, R.C., Lanza, N.L., 2023. Acoustics and LIBS profiling of soils at Jezero crater, Mars. In: LPI Contributions, vol. 2806, p. 1521.

Maurice, S., Wiens, R.C., Bernardi, P., Caïs, P., Robinson, S., Nelson, T., Gasnault, O., Reess, J.-M., Deleuze, M., Rull, F., et al., 2021. The SuperCam instrument suite on the Mars 2020 rover: Science objectives and mast-unit description. Space Sci. Rev. 217 (3), 1–108.

Maurice, S., Wiens, R.C., Saccoccio, M., Barraclough, B., Gasnault, O., Forni, O., Mangold, N., Baratoux, D., Bender, S., Berger, G., Bernardin, J., Berthé, M., Bridges, N., Blaney, D., Bouyé, M., Caïs, P., Clark, B., Clegg, S., Cousin, A., Cremers, D., Cros, A., DeFlores, L., Derycke, C., Dingler, B., Dromart, G., Dubois, B., Dupieux, M., Durand, E., d'Uston, L., Fabre, C., Faure, B., Gaboriaud, A., Gharsa, T., Herkenhoff, K., Kan, E., Kirkland, L., Kouach, D., Lacour, J.L., Langevin, Y., Lasue, J., Le Mouélic, S., Lescure, M., Lewin, E., Limonadi, D., Manhès, G., Mauchien, P., McKay, C., Meslin, P.Y., Michel, Y., Miller, E., Newsom, H.E., Orttner, G., Paillet, A., Parès, L., Parot, Y., Pérez, R., Pinet, P., Poitrasson, F., Quertier, B., Sallé, B., Sotin, C., Sautter, V., Séran, H., Simmonds, J.J., Sirven, J.B., Stiglich, R., Striebig, N., Thocaven, J.J., Toplis, M.J., Vaniman, D., 2012. The ChemCam instrument suite on the Mars Science Laboratory (MSL) rover: Science objectives and mast unit description. Space Sci. Rev. 170 (1–4), 95–166. http://dx.doi.org/10.1007/s11214-012-9912-2.

McSween, Jr., H.Y., McGlynn, I.O., Rogers, A.D., 2010. Determining the modal mineralogy of Martian soils. J. Geophys. Res.: Planets 115 (E7), http://dx.doi.org/10.1029/2010JE003582.

Meslin, P.Y., Forni, O., Beck, P., Cousin, A., Beyssac, O., Lopez-Reyes, G., Benzerara, K., Ollila, A., Mandon, L., Wiens, R.C., Clegg, S., Montagnac, G., Clavé, E., Manrique, J.A., Chide, B., Maurice, S., Gasnault, O., Lasue, J., Quantin-Nataf, C., Dehouck, E., Sharma, S.K., Arana, G., Madariaga, J.M., Castro, K., Schröder, S., Mangold, N., Poulet, F., Johnson, J., Le Mouélic, S., Zorzano, M.P., 2022. Evidence for Perchlorate and Sulfate Salts in Jezero Crater, Mars, from Supercam Observations. In: 53rd Lunar and Planetary Science Conference. In: LPI Contributions, vol. 2678, p. 2694.

Meslin, P.-Y., Forni, O., Beck, P., Cousin, A., Beyssac, O., Lopez-Reyes, G., Benzerara, K., Ollila, A., Mandon, L., Wiens, R., et al., 2022. Evidence for perchlorate and sulfate salts in Jezero crater, Mars, from supercam observations. In: Lunar and Planetary Science Conference, vol. 53, p. 2694.

Meslin, P.-Y., Gasnault, O., Forni, O., Schröder, S., Cousin, A., Berger, G., Clegg, S., Lasue, J., Maurice, S., Sautter, V., et al., 2013. Soil diversity and hydration as observed by ChemCam at Gale crater, Mars. Science 341 (6153), 1238670.

Ming, D.W., Gellert, R., Morris, R.V., Arvidson, R.E., Brückner, J., Clark, B.C., Cohen, B.A., d'Uston, C., Economou, T., Fleischer, I., Klingelhöfer, G., McCoy, T.J., Mittlefehldt, D.W., Schmidt, M.E., Schröder, C., Squyres, S.W., Tréguier, E., Yen, A.S., Zipfel, J., 2008. Geochemical properties of rocks and soils in gusev crater, Mars: Results of the alpha particle X-Ray spectrometer from cumberland ridge to home plate. J. Geophys. Res.: Planets 113 (E12), http://dx.doi.org/10.1029/2008JE003195.

Nachon, M., Mangold, N., Forni, O., Kah, L.C., Cousin, A., Wiens, R.C., Anderson, R., Blaney, D., Blank, J.G., Calef, F., Clegg, S.M., Fabre, C., Fisk, M.R., Gasnault, O., Grotzinger, J.P., Kronyak, R., Lanza, N.L., Lasue, J., Le Deit, L., Mouélic, S.L., Maurice, S., Meslin, P.Y., Oehler, D.Z., Payré, V., Rapin, W., Schröder, S., Stack, K., Sumner, D., 2017. Chemistry of diagenetic features analyzed by ChemCam at Pahrump Hills, Gale crater, Mars. Icarus 281, 121–136. http://dx.doi.org/10.1016/j.icarus.2016.08.026.

O'Connell-Cooper, C.D., Spray, J.G., Thompson, L.M., Gellert, R., Berger, J.A., Boyd, N.I., Desouza, E.D., Perrett, G.M., Schmidt, M., VanBommel, S.J., 2017. APXS-derived chemistry of the Bagnold dune sands: Comparisons with Gale crater soils and the global Martian average. J. Geophys. Res.: Planets 122 (12), 2623–2643. http://dx.doi.org/10.1002/2017JE005268.

Payré, V., Siebach, K., Dasgupta, R., Udry, A., Rampe, E., Morrison, S., 2020. Constraining ancient magmatic evolution on Mars using crystal chemistry of detrital igneous minerals in the sedimentary Bradbury group, Gale crater, Mars. J. Geophys. Res.: Planets 125 (8), e2020JE006467.

Phua, Y., Ehlmann, B.L., Mandon, L., Siljeström, S., Razzell Hollis, J., Bhartia, R., 2023. Characterizing hydration in alteration minerals of Jezero crater geologic units with SHERLOC on Mars-2020. In: LPI Contributions, vol. 2806, p. 1392.

Polkko, J., Hieta, M., Harri, A.-M., Tamppari, L., Martínez, G., Viúdez-Moreiras, D., Savijärvi, H., Conrad, P., Zorzano Mier, M.P., De La Torre Juarez, M., Hueso, R., Munguira, A., Leino, J., Gómez, F., Jaakonaho, I., Fischer, E., Genzer, M., Apestigue, V., Arruego, I., Banfield, D., Lepinette, A., Paton, M., Rodriguez-Manfredi, J.A., Sánchez Lavega, A., Sebastian, E., Toledo, D., Vicente-Retortillo, A., MEDA team, 2023. Initial results of the relative humidity observations by MEDA instrument onboard the Mars 2020 perseverance rover. J. Geophys. Res.: Planets 128 (2), http://dx.doi.org/10.1029/2022JE007447, e2022JE007447.

Pommerol, A., Schmitt, B., 2008a. Strength of the H2O near-infrared absorption bands in hydrated minerals: Effects of measurement geometry. J. Geophys. Res.: Planets 113 (E12), http://dx.doi.org/10.1029/2008JE003197.

Pommerol, A., Schmitt, B., 2008b. Strength of the H2O near-infrared absorption bands in hydrated minerals: Effects of particle size and correlation with albedo. J. Geophys. Res.: Planets 113 (E10), http://dx.doi.org/10.1029/2007JE003069.

Pommerol, A., Schmitt, B., Beck, P., Brissaud, O., 2009. Water sorption on Martian regolith analogs: Thermodynamics and near-infrared reflectance spectroscopy. Icarus (ISSN: 0019-1035) 204 (1), 114–136. http://dx.doi.org/10.1016/j.icarus.2009.06.013.

Prepared by the MSR Campaign Science Group (MCSG), Czaja, A.D., Zorzano, M.-P., the rest of the MCSG team, w.C., Kminek, G., Meyer, M.A., Members, Beaty, D.W., Sefton-Nash, E., Carrier, B.L., Thiessen, F., Haltigin, T., Bouvier, A., Dauphas, N., French, K.L., Hallis, L.J., Harris, R.L., Hauber, E., Rodriguez, L.E., Schwenzer, S.P., Steele, A., Tait, K.T., Thorpe, M.T., Usui, T., Vanhomwegen, J., Velbel, M.A., Edwin, S., Farley, K.A., Glavin, D.P., Harrington, A.D., Hays, L.E., Hutzler, A., Wadhwa, M., 2023. Report of the science community workshop on the proposed first sample depot for the Mars sample return campaign. Meteorit. Planet. Sci. 58 (6), 885–896. http://dx.doi.org/10.1111/maps.13981.

Rampe, E., Blake, D., Bristow, T., Ming, D., Vaniman, D., Morris, R., Achilles, C., Chipera, S., Morrison, S., Tu, V., Yen, A., Castle, N., Downs, G., Downs, R., Grotzinger, J., Hazen, R., Treiman, A., Peretyazhko, T., Des Marais, D., Walroth, R., Craig, P., Crisp, J., Lafuente, B., Morookian, J., Sarrazin, P., Thorpe, M., Bridges, J., Edgar, L., Fedo, C., Freissinet, C., Gellert, R., Mahaffy, P., Newsom, H., Johnson, J., Kah, L., Siebach, K., Schieber, J., Sun, V., Vasavada, A., Wellington, D., Wiens, R., 2020. Mineralogy and geochemistry of sedimentary rocks and eolian sediments in Gale crater, Mars: A review after six earth years of exploration with Curiosity. Geochemistry (ISSN: 0009-2819) 80 (2), 125605. http://dx.doi.org/10.1016/j.chemer.2020.125605.

Rampe, E., Lapotre, M., Bristow, T., Arvidson, R., Morris, R., Achilles, C., Weitz, C., Blake, D., Ming, D., Morrison, S., et al., 2018. Sand mineralogy within the Bagnold Dunes, Gale crater, as observed in situ and from orbit. Geophys. Res. Lett. 45 (18), 9488–9497.

Rapin, W., Bousquet, B., Lasue, J., Meslin, P.-Y., Lacour, J.-L., Fabre, C., Wiens, R., Frydenvang, J., Dehouck, E., Maurice, S., Gasnault, O., Forni, O., Cousin, A., 2017a. Roughness effects on the hydrogen signal in laser-induced breakdown spectroscopy. Spectrochim. Acta B: Atom. Spectrosc. (ISSN: 0584-8547) 137, 13–22. http://dx.doi.org/10.1016/j.sab.2017.09.003.

Rapin, W., Dromart, G., Rubin, D., Le Deit, L., Mangold, N., Edgar, L.A., Gasnault, O., Herkenhoff, K., Le Mouélic, S., Anderson, R., et al., 2021. Alternating wet and dry depositional environments recorded in the stratigraphy of Mount Sharp at Gale crater, Mars. Geology 49 (7), 842–846.

Rapin, W., Ehlmann, B., Dromart, G., Schieber, J., Thomas, N., Fischer, W., Fox, V., Stein, N., Nachon, M., Clark, B., Kah, L., Thompson, L., Meyer, H., Gabriel, T., Hardgrove, C., Mangold, N., Rivera-Hernandez, F., Wiens, R., Vasavada, A., 2019. An interval of high salinity in ancient Gale crater lake on Mars.

Rapin, W., Meslin, P.-Y., Maurice, S., Wiens, R.C., Laporte, D., Chauviré, B., Gasnault, O., Schröder, S., Beck, P., Bender, S., et al., 2017b. Quantification of water content by laser induced breakdown spectroscopy on Mars. Spectrochim. Acta B: Atomic Spectrosc. 130, 82–100.

Rogers, A.D., Aharonson, O., 2008. Mineralogical composition of sands in Meridiani Planum determined from Mars exploration rover data and comparison to orbital measurements. J. Geophys. Res.: Planets 113 (E6), http://dx.doi.org/10.1029/2007JE002995.

Royer, C., Bedford, C.C., Wiens, R.C., Johnson, J.R., Horgan, B.H., Broz, A., Forni, O., Connell, S., Mandon, L., Kathir, B.S., Hausrath, E.M., Udry, A., Madariaga, J.M., Dehouck, E., Anderson, R.B., Beck, P., Beyssac, O., Clavé, E., Clegg, S.M., Cloutis, E., Fouchet, T., Gabriel, T.S., Garczynski, B.J., Klidaras, A., Manelski, H.T., Mayhew, L., Nunez, J., Ollila, A.M., Schroder, S., Simon, J.I., Wolf, U., Morgan, K.M., Cousin, A., Maurice, S., 2024. Mineral composition of Al-rich float rocks in Jezero crater as seen by SuperCam. In: LPI Contributions, vol. 3040, p. 1371.

Royer, C., Fouchet, T., Mandon, L., Montmessin, F., Poulet, F., Forni, O., Johnson, J.R., Legett, C., Le Mouélic, S., Gasnault, O., Quantin-Nataf, C., Beck, P., Dehouck, E., Clavé, E., Ollila, A.M., Pilorget, C., Bernardi, P., Reess, J.M., Pilleri, P., Brown, A., Newell, R.T., Cloutis, E., Maurice, S., Wiens, R.C., 2023. Reflectance of Jezero crater floor: 1. Data processing and calibration of the infrared spectrometer (IRS) on SuperCam. J. Geophys. Res. (Planets) 128 (1), http://dx.doi.org/10.1029/2022JE007481, e2022JE007481.

Royer, C., Poulet, F., Reess, J.-M., Pilorget, C., Hamm, V., Fouchet, T., Maurice, S., Forni, O., Bernardi, P., Montmessin, F., Lapauw, L., Parisot, J., Bonafous, M., Gasnault, O., Wiens, R.C., 2020. Pre-launch radiometric calibration of the infrared spectrometer onboard SuperCam for the Mars2020 rover. Rev. Sci. Instrum. 91 (6), 063105. http://dx.doi.org/10.1063/1.5145390.

Sagan, C., Pieri, D., Fox, P., Arvidson, R.E., Guinness, E.A., 1977. Particle motion on Mars inferred from the viking lander cameras. J. Geophys. Res. (1896-1977) 82 (28), 4430–4438. http://dx.doi.org/10.1029/JS082i028p04430.

Sautter, V., Toplis, M., Wiens, R., Cousin, A., Fabre, C., Gasnault, O., Maurice, S., Forni, O., Lasue, J., Ollila, A., et al., 2015. In situ evidence for continental crust on early Mars. Nat. Geosci. 8 (8), 605–609.

Savijärvi, H., Harri, A.-M., 2021. Water vapor adsorption on Mars. Icarus (ISSN: 0019-1035) 357, 114270. http://dx.doi.org/10.1016/j.icarus.2020.114270.

Sullivan, R.J., Cabrol, N.A., Golombek, M., Herkenhoff, K.E., Landis, G., Mer Athena Science Team, 2010. Aeolian grain evolution on Mars: Implications for regolith origins. In: AGU Fall Meeting Abstracts, vol. 2010, pp. P53A–1489.

Sultana, R., Poch, O., Beck, P., Schmitt, B., Quirico, E., 2021. Visible and near-infrared reflectance of hyperfine and hyperporous particulate surfaces. Icarus 357, 114141.

Sun, V.Z., Hand, K.P., Stack, K.M., Farley, K.A., Simon, J.I., Newman, C., Sharma, S., Liu, Y., Wiens, R.C., Williams, A.J., Tosca, N., Alwmark, S., Beyssac, O., Brown, A., Calef, F., Cardarelli, E.L., Clavé, E., Cohen, B., Corpolongo, A., Czaja, A.D., Del Sesto, T., Fairen, A., Fornaro, T., Fouchet, T., Garczynski, B., Gupta, S., Herd, C.D.K., Hickman-Lewis, K., Horgan, B., Johnson, J., Kinch, K., Kizovski, T., Kronyak, R., Lange, R., Mandon, L., Milkovich, S., Moeller, R., Núñez, J., Paar, G., Pyrzak, G., Quantin-Nataf, C., Shuster, D.L., Siljestrom, S., Steele, A., Tice, M., Toupet, O., Udry, A., Vaughan, A., Wogsland, B., 2023. Overview and results from the Mars 2020 perseverance Rover's first science campaign on the Jezero crater floor. J. Geophys. Res.: Planets 128 (6), http://dx.doi.org/10.1029/2022JE007613, e2022JE007613 2022JE007613.

Udry, A., Ostwald, A., Sautter, V., Cousin, A., Beyssac, O., Forni, O., Dromart, G., Benzerara, K., Nachon, M., Horgan, B., et al., 2022. A Mars 2020 perseverance SuperCam perspective on the igneous nature of the Máaz formation at Jezero crater and link with Séítah, Mars. J. Geophys. Res.: Planets e2022JE007440.

Vakkada Ramachandran, A., Zorzano, M.-P., Martín-Torres, J., 2021. Experimental investigation of the atmosphere-regolith water cycle on present-day Mars. Sensors (ISSN: 1424-8220) 21 (21), http://dx.doi.org/10.3390/s21217421.

Van Es, H., 2017. A new definition of soil. CSA News 62 (10), 20–21. http://dx.doi.org/10.2134/csa2017.62.1016.

Vaughan, A., Minitti, M.E., Cardarelli, E.L., Johnson, J.R., Kah, L.C., Pilleri, P., Rice, M.S., Sephton, M., Horgan, B.H., Wiens, R.C., et al., 2023. Regolith of the crater floor units, Jezero crater, Mars: Textures, composition, and implications for provenance. J. Geophys. Res.: Planets 128 (3), e2022JE007437.

Viviano, C.E., Seelos, F.P., Murchie, S.L., Kahn, E.G., Seelos, K.D., Taylor, H.W., Taylor, K., Ehlmann, B.L., Wiseman, S.M., Mustard, J.F., et al., 2014. Revised CRISM spectral parameters and summary products based on the currently detected mineral diversity on Mars. J. Geophys. Res.: Planets 119 (6), 1403–1431.

Wentworth, C.K., 1922. A scale of grade and class terms for clastic sediments. J. Geol. 30 (5), 377–392.

Wiens, R.C., Maurice, S., Barraclough, B., Saccoccio, M., Barkley, W.C., Bell, J.F., Bender, S., Bernardin, J., Blaney, D., Blank, J., Bouyé, M., Bridges, N., Bultman, N., Caïs, P., Clanton, R.C., Clark, B., Clegg, S., Cousin, A., Cremers, D., Cros, A., DeFlores, L., Delapp, D., Dingler, R., D'Uston, C., Darby Dyar, M., Elliott, T., Enemark, D., Fabre, C., Flores, M., Forni, O., Gasnault, O., Hale, T., Hays, C., Herkenhoff, K., Kan, E., Kirkland, L., Kouach, D., Landis, D., Langevin, Y., Lanza, N., LaRocca, F., Lasue, J., Latino, J., Limonadi, D., Lindensmith, C., Little, C., Mangold, N., Manhes, G., Mauchien, P., McKay, C., Miller, E., Mooney, J., Morris, R.V., Morrison, L., Nelson, T., Newsom, H., Ollila, A., Ott, M., Pares, L., Perez, R., Poitrasson, F., Provost, C., Reiter, J.W., Roberts, T., Romero, F., Sautter, V., Salazar, S., Simmonds, J.J., Stiglich, R., Storms, S., Striebig, N., Thocaven, J.-J., Trujillo, T., Ulibarri, M., Vaniman, D., Warner, N., Waterbury, R., Whitaker, R., Witt, J., Wong-Swanson, B., 2012. The ChemCam instrument suite on the Mars Science Laboratory (MSL) Rover: Body unit and combined system tests. Space Sci. Rev. 170 (1–4), 167–227. http://dx.doi.org/10.1007/s11214-012-9902-4.

Wiens, R.C., Maurice, S., Robinson, S.H., Nelson, A.E., Cais, P., Bernardi, P., Newell, R.T., Clegg, S., Sharma, S.K., Storms, S., et al., 2021. The SuperCam instrument suite on the NASA Mars 2020 rover: Body unit and combined system tests. Space Sci. Rev. 217 (1), 1–87.

Wiens, R.C., Udry, A., Beyssac, O., Quantin-Nataf, C., Mangold, N., Cousin, A., Mandon, L., Bosak, T., Forni, O., McLennan, S.M., et al., 2022. Compositionally and density stratified igneous terrain in Jezero crater, Mars. Sci. Adv. 8 (34), eabo3399.

Williams, A.J., Russell, P., Sun, V.Z., Shuster, D.L., Stack-Morgan, K.M., Farley, K.A., del Sesto, T., Kronyak, R.E., Bell, J.F., Beyssac, O., et al., 2023. Exploring the Jezero Delta front: Overview of results from the Mars 2020 perseverance rover's second science campaign. In: 54th Lunar and Planetary Science Conference, vol. 54, p. 1652.

Yen, A., Gellert, R., Schroeder, C., Morris, R., Bell, J., Knudson, A., Clark, B., Ming, D., J. Crisp, R.A., Blaney, D., Bruckner, J., Christensen, P., DesMarais, D., Souza, P.D., Economou, T., Ghosh, A., Hahn, B., Herkenhoff, K., Haskin, L., Hurowitz, J., Joliff, B., Johnson, J., Klingelhofer, G., Badsen, M., McLennan, S., McSewwen, H., Richter, L., Rieder, R., Rodionov, D., Soderblom, L., Squyres, S., Tosca, N., Wang, A., Wyatt, M., Zipfel, J., 2005. An integrated view of the chemistry and mineralogy of Martian soils. Nature 436, http://dx.doi.org/10.1038/nature03637.

Zent, A.P., Quinn, R.C., 1997. Measurement of H2O adsorption under Mars-like conditions: Effects of adsorbent heterogeneity. J. Geophys. Res.: Planets 102 (E4), 9085–9095. http://dx.doi.org/10.1029/96JE03420.